From Burial to Barrier: How burial history controls the hydraulic conductivity in argillaceous formations

Raphael Burchartz[1,2*], Brian Mutuma Mbui[3], Peter Achtziger-Zupančič[4], Garri Gaus[3,4], Timo Seemann[1], Lisa Winhausen[1], Yvonne Spychala[2], Mohammadreza Jalali[1], Ralf Littke[2] & Florian Amann[1, 4]

[1]Institute of Engineering Geology and Hydrogeology, RWTH-Aachen University, Aachen, Germany
[2]Geological institute, RWTH-Aachen University, Aachen, Germany
[3]Institute of Organic Biogeochemistry in Geo-Systems, RWTH-Aachen University, Aachen, Germany
[4] Fraunhofer Research Institution for Energy Infrastructures and Geotechnologies IEG, 52056 Aachen, Germany

Correspondence to: Raphael Burchartz (burchartz@lih.rwth-aachen.de)

Abstract Deep geological repositories for high-level radioactive waste (HLW) rely to a large extent~~d~~ on the long-term sealing~~hydraulic~~ integrity of host rocks to limit fluid flow and radionuclide migration. Low hydraulic conductivity ($K<10^{-10}$ m/s; StandAG, 2017) is a key factor for effective long-term barrier performance~~, and~~. Among other properties, argillaceous formations are promising candidates due to their ~~strong~~ effective aquitard characteristics. However, predicting their bulk hydraulic behaviour across temporal and spatial scales remains difficult, as it reflects the combined effects of intrinsic material properties and post-depositional evolution. This study compiles 782 hydraulic conductivity measurements from six European argillaceous formations, including laboratory and field scales. By integrating petrophysical, mineralogical, and reconstructed burial history data, we identify systematic links between burial evolution and hydraulic behaviour. Results show that maximum burial depth and associated stress and temperature conditions ~~exert~~ emerge as a primary and consistent~~first-order~~ control on matrix-scale hydraulic conductivity, which is largely retained after uplift. In contrast, bulk hydraulic behaviour at the rock-mass scale reflects interactions between maximum burial depth and present-day depth, ~~defining~~ as controlled by processes such as decompaction, fracturing, and self-sealing processes. Three evolutionary trends emerge from the compiled data: (1) Shallowly buried (<400 m), poorly indurated formations show limited hydraulic variability and scale independence; (2) Moderately buried (~85~~80~~0 m – 2,000 m), over-consolidated (stiff clay) formations retain low matrix hydraulic conductivity after uplift, but exhibit gradually (partly significantly) enhanced hydraulic conductivity at depths <100 m due to the evolution of a pronounced decompaction zone. When devoted to less pronounced uplift and at greater present-day depths (>250 m) matrix and bulk hydraulic conductivities converge and predominantly range within a natural variability between 10^{-14} to 10^{-12} m/s, indicating effective self-sealing processes; (3) deeply buried formations (>2,000 m) become increasingly indurated and brittle, with reduced self-sealing capacity due to the loss of swellable clay mineral phases and fracture-dominated bulk hydraulic behaviour. Matrix and rock-mass hydraulic conductivities may diverge by several orders of magnitude. These trends provide predictive insights into the long-term barrier performance of argillaceous host rocks in HLW repositories.

Formatiert: Abstand Nach: 0 Pt., Rahmen: Oben: (Kein Rahmen), Unten: (Kein Rahmen), Links: (Kein Rahmen), Rechts: (Kein Rahmen)

1 Introduction

Argillaceous geo-materials, such as consolidated clays, claystones, and shales, are widely recognized as potential host rocks and natural barriers for the permanent disposal of high-level radioactive waste (HLW) in deep

geological repositories (DGRs) (Delage et al., 2010; Norris, 2017). Their favorable properties, including extremely low permeability (often in the range of micro- to nano-Darcy), self-sealing behaviour of fractures, and strong sorption capacity, provide favorable conditions for the safe long-term containment of hazardous radionuclides generated by the radioactive decay of waste products (Bock et al., 2010; Delage et al., 2010; Mazurek et al., 2011; OECD and NEA, 2022).

Fluid-flow within argillaceous formations is a key determinant of their sealing efficiency, as it largely governs solute transport (Patriarche et al., 2004a). Hence, assessing the long-term barrier effectiveness of these formations requires a detailed understanding of their hydrogeological properties, particularly transport characteristics such as permeability (k) or hydraulic conductivity (K). While permeability (k, m^2) is a measure of the intrinsic ability of a material to transmit fluids, hydraulic conductivity (K, m/s) reflects both the permeability and fluid properties (viscosity and density), and is more commonly reported in hydrogeological applications and therefore taken as the convention used in this study. Following Darcy´s law the hydraulic conductivity can be expressed as

$$K = \frac{Q*L}{A*\Delta h} \quad (1)$$

where Q (m^3/s) is the total volumetric flow rate, L (m) is the length of the flow path, A (m^2) is the cross sectional area, and Δh is the hydraulic head difference.

In intact (unfractured) argillaceous rock, hydraulic conductivity is exceptionally low (mostly $<10^{-12}$ m/s), significantly restricting advective flow and making diffusion the dominant transport mechanism (Mazurek et al., 2011). At the rock-mass scale, hydraulic conductivity may be increasingly governed by fracture networks that are superimposed on the low-permeable matrix. However, characterizing and quantifying fluid transmission in these formations remains a major challenge due to the time-intensive nature of measurement techniques (Boisson et al., 2001; Yang and Aplin, 2007; Neuzil, 2019; Winhausen et al., 2020) and the potentially strong spatial ~~anisotropy~~ variability of hydraulic properties, which can vary across different scales, ~~partly~~ by up to several orders of magnitude (Yu et al., 2017). This ~~anisotropy~~ variability reflects both anisotropy (directional dependence of hydraulic properties, arising primarily from the orientation of bedding/stratification) ~~arises from multiple factors, including orientation of the bedding/stratification~~ (Aertsens et al., 2004; Yang and Aplin, 2007), and heterogeneity, e.g., spatial variability arising from ~~the presence of~~ secondary fluid pathways such as fractures, ~~and~~ sedimentological ~~heterogeneities~~differences ~~in sedimentological~~, ~~i.e.~~ (e.g., grain-size variations and their distribution), and mineralogical facies~~, i.e.~~ (e.g. clay mineral content and type) (Dewhurst et al., 1998, 1999; Yang and Aplin, 2007). Hence, methodological factors such as the scale of investigation, the orientation of specimens with respect to the bedding, or the ~~applied~~ method of testing used ~~become~~ are crucial determinants in the assessment of transport characteristics of argillaceous formations and need consideration in modelling approaches.

An important factor shaping the hydraulic characteristics of argillaceous formations is their burial history, including the associated stress states (dictated by the interplay of overburden, pore fluid pressure, tectonic stresses and the resulting effective stress) and temperature conditions. ~~An important factor shaping the hydraulic characteristics of argillaceous formations is their burial history, including the past associated stress and temperature conditions.~~ In general, the hydraulic conductivity of argillaceous formations is closely linked to the pore space accessible for fluid flow ~~and~~ which decreases logarithmically with pore closure and increasing

Formatiert: Hochgestellt

Formatiert: Hochgestellt

tortuosity of flow paths during gradual burial, induced by mechanical compaction and chemical cementation (Neuzil, 1994; Yang and Aplin, 2007; Mazurek et al., 2011; Carcione et al., 2019). After the deposition of clay-rich muds, compaction and consolidation processes may reduce the permeability by six or more orders of magnitude, reaching values as low as 10^{-23} m^2 (Neuzil, 2019). During mechanical compaction, most pronounced at shallow to intermediate burial depths (typically between 0 m and 2,000 m to 3,000 m), the reduction in porosity, and consequently pore water flux, is directly driven by the progressive increase in effective stress and strength of the sediment grain framework (Athy, 1930; Bjørlykke, 1999; Avseth et al., 2001; Ewy et al., 2020). With increasing depth and at ~~higher~~ temperatures exceeding ~~(>~~70 – 80°C~~)~~, mineral alteration and cementation become dominant diagenetic processes. Cementation by precipitation of minerals around the clastic grains will result in further porosity loss and consequently in reduced fluid flow through the rock matrix (Bjørlykke, 1999, 2014). However, progressive porosity reduction during burial may be counteracted by undercompaction, whereby the low-permeability clay matrix restricts fluid expulsion and consequently leads to the development of excess pore pressures (Bowers, 1995; Swarbrick and Osborne, 1998; Hart et al., 2023; Castro-Vera et al., 2024; Burchartz et al., 2026).

Initially, poorly consolidated argillaceous muds ~~present~~ possess a high grade of plasticity, resulting in the ability to undergo substantial deformation without exhibiting ~~prominent~~ significant fracturing (Horseman et al., 1987, 1996). However, the gradual burial and heating of initially ductile muds, accompanied by mechanical compaction and the precipitation of cementing minerals, can progressively increase the brittleness of the material. The transition from ductile to brittle behaviour occurs at varying depths and temperatures, depending on the mineralogical composition and textural relationships (Bjørlykke and Høeg, 1997). ~~As a result of uplift-induced decompaction, or non-hydrostatic stress conditions (e.g., related to fluid overpressure), the rock might experience ductile or brittle deformation (Bjørlykke and Høeg, 1997).~~ In the brittle regime, deformation typically results in the formation of dilatant features such as fractures and faults, which can locally enhance hydraulic conductivity and fluid transport properties, potentially compromising the sealing capacity of the formation (Ishii et al., 2011). Upon deep burial at high confining stresses and associated elevated temperatures, brittle fracturing can be suppressed by increasing ductility at grain-scale deformations (Winhausen et al., 2022).

Following deep burial, many formations considered as potential HLW host rocks have undergone significant uplift due to tectonic processes and/or erosion of overlying strata. This uplift results in over-consolidation of the formation (present effective stress < past effective stress), whereby the rock matrix retains a memory of its maximum past burial stress. Over-consolidation can substantially alter the hydro-mechanical properties as it enhances shear strength and brittleness of argillaceous formations (Wagner, 2013; Winhausen et al., 2022). ~~Additionally, the uplift-related~~As a result of uplift, the stress relief typically promotes the formation of discontinuities or fracturing, ultimately leading to the development of a pronounced decompaction zone (Einsele et al., 1985; Hekel, 1994; Czerewko and Cripps, 2006), in which increased fracture susceptibility may lead to locally enhanced transport properties (Hekel, 1994; Vogt et al., 2017; Gautschi, 2017).

Understanding the complex interplay of burial history, including processes such as mechanical compaction, cementation, mineral alteration, and uplift-related decompaction, and their cumulative effects on hydraulic behaviour is essential for evaluating the long-term integrity of argillaceous host rocks. Equally important is

recognizing how technical variability in testing methods, such as differences between laboratory and *in situ* scales or variations in packer interval length, can influence measured hydraulic conductivity values. Both, geological evolution and methodological choices must be carefully considered to ensure robust assessment of hydraulic performance in these formations.

To address this, the present study compiles and analyses a comprehensive dataset of hydraulic conductivity measurements from both laboratory and field investigations across six European clay-rich formations currently under consideration for HLW disposal (Fig. 1): the Aalenian Opalinus Clay Formation (Switzerland and Germany), the Callovo-Oxfordian (~~CO~~France) and Toarcian-Domerian (~~To Do~~France) Argillites ~~(France)~~, the Pliensbachian Amaltheenton Formation (Germany), the Rupelian Boom Clay (Belgium), and the Upper Permian Boda Claystone Formation (~~BCF~~Hungary).

These formations represent a paragenetic sequence that spans early diagenetic, ductile clays (eogenesis), through mid-diagenetic claystones (mesogenesis), to late-diagenetic, deeply buried and brittle claystones that have undergone significant uplift and thus exhibit pronounced over-consolidation. Special emphasis is placed on linking their hydraulic characteristics to the respective diagenetic evolution and burial history, as well as to mineralogical properties and methodological factors such as the investigation scale. By integrating these aspects, this study aims to contribute to a more robust understanding of the long-term hydrogeological performance of argillaceous formations as host rocks for deep geological repositories.

2 Studied Formations and Sites

The argillaceous formations considered in this study are briefly described in the subsequent sections. Some formations are represented by data from multiple sampling and testing sites (Fig. 1). Geological, petrophysical, mechanical, and mineralogical properties of all formations, except the Amaltheenton Formation, are summarized in the 2022 Clay Club Catalogue (CCC) database, published by the OECD & NEA (2022). Data for the Amaltheenton Formation, not included in the CCC, is derived from investigations undertaken as part of the MATURITY project (Burchartz et al., 2026). Table 1 presents key formation properties as given in the CCC and by ~~(~~Burchartz et al.~~,~~ (2026) and~~;~~ Mbui et al.~~,~~ (2026)~~.~~ ~~Burchartz et al. (2025).~~

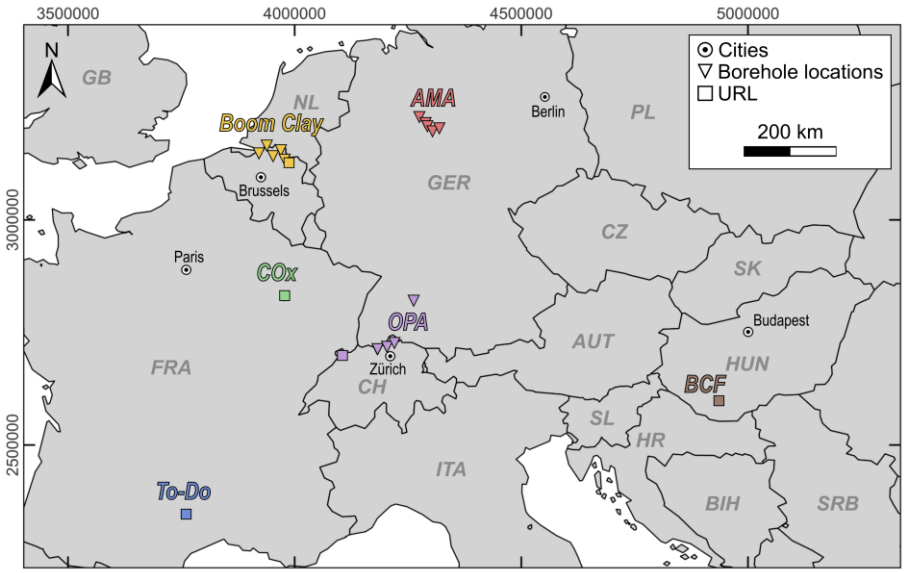


Figure 1 Formations and their locations in central Europe that served as data for this study. Boom Clay, OPA=Opalinus Clay Formation, COx=Callovo-Oxfordian Argillite, To-Do=Domerian-Toarcian Argillite, AMA=Amaltheenton Formation, BCF=Boda Claystone Formation, URL=Undergorund Research Laboratory.

2.1 Boom Clay Formation (Boom)

The Boom Clay Formation in northeastern Belgium was deposited during the Lower Oligocene (Rupelian) in a shallow marine environment of the North Sea Basin, at estimated paleo-depths of 50–100 m (Vandenberghe and Mertens, 2013; Zeelmaekers et al., 2015). It comprises rhythmically alternating clay-rich and silt-rich beds (Dehandschutter et al., 2005), subdivided into three stratigraphic members: the Belsele-Waas Member (siltiest), the Terhagen Member (pale grey clay, lowest coarse fraction), and the Putte Member (organic-rich dark clays) (Aertsens et al., 2004). ~~Present-day formation top depths range from ~50 to 260 m, with a thickness between 80 and 100 m.~~ Mineralogically, the formation is considered homogeneous, containing ~60 wt.% clay minerals dominated by illite, with subordinate smectite, kaolinite, chlorite, ~20 wt.% quartz, and ~10 wt.% feldspar (Aertsens et al., 2004; Frederickx et al., 2018, 2021). Its burial history includes continuous subsidence, interrupted by a minor uplift phase during the Chattian, resulting in a modest over-consolidation ratio (OCR) of ~2.4 (OECD and NEA, 2022).

Hydraulic conductivity data compiled for this study originate primarily from boreholes in northeastern Belgium (Essen-1, Zoersel, Weelde-1, Doel-2b, Mol-1) and the HADES Underground Research Laboratory (URL) in Mol. In these locations, p~~P~~resent-day formation top depths range from ~50 to 260 m, and the Boom Clay shows ~~with a~~ thicknesses between 80 and 100 m. Most laboratory measurements were obtained using ~~pulse or~~ constant-head permeameter tests and diffusion/migration experiments, while *in situ* data, exclusively from piezometers, were collected in URL-drilled boreholes. In total, 269 laboratory and 30 *in situ* measurements were evaluated, yielding a hydraulic conductivity range of 3.5×10^{-10} to 2.1×10^{-13} m/s.

Formatiert: Schriftart: Kursiv

Formatiert: Schriftart: Kursiv

2.2. Amaltheenton Formation (AMA)

The Amaltheenton Formation, deposited under shallow-marine conditions during the Upper Pliensbachian in the Lower Saxony Basin (~~LSB,~~ Germany), consists predominantly of organic-lean, grey claystones and calcareous claystones, frequently intersected by siderite concretions. Formation thicknesses between 100 and 200 m have been inferred from borehole profiles and outcrop data (Burnaz et al., 2024; Marten et al., 2024; Wijesinghe et al., 2025). In the Hils and Sack synclines of Lower Saxony, the formation experienced highly variable maximum burial depths, ranging from approximately 1,300 to 3,300 m over a SE–NW transect of ~50 km (Castro-Vera et al., 2024; Burchartz et al., 2026). Cretaceous inversion tectonics resulted in substantial uplift to shallow depths (from few metres to several decametres below the surface with respect to the formation top) and pronounced over-consolidation (Stahl, 1993; Voigt et al., 2021; Gaus et al., 2022). As no directly measured OCR values are available for AMA, we estimate a conservative OCR>20 from the ratio of reconstructed maximum burial depth to present-day depth, assuming hydrostatic pore pressure conditions.

Within the MATURITY project, eight boreholes were drilled across five locations, intercepting the AMA at variable depths (formation tops between 2 and 74 metres below ground surface (mbgs)) and formation thicknesses, capturing the full extent of the lateral burial variability. A comprehensive investigation campaign was carried out, involving both laboratory and in-situ testing. Laboratory hydraulic conductivity data is based on permeameter experiments while *in situ* data stems from hydraulic testing conducted using straddle-packer systems in both single- and double-packer configurations (Burchartz et al., 2026)~~(Burchartz et al., 2025)~~.

The mineralogical composition of the AMA is similar across the study area, with total clay mineral contents ranging from 58 to 75 wt.%, framework silicates between 7 and 23 wt.%, and carbonates from 1 to 8 wt.% (Burchartz et al., 2026). Laboratory-derived hydraulic conductivities fall between $1.8 \times$ ~~x~~10^{-12} and $1.3 \times$ ~~x~~10^{-13} m/s, while in-situ measurements indicate significantly higher values, ranging from $3.4 \times$ ~~x~~10^{-5} to $1.1 \times$ ~~x~~10^{-7} m/s, reflecting the influence of fractures, stress relief, or testing-related disturbances (Burchartz et al., 2026).

2.3 Toarcian-Domerian Argillite (To-Do)

Toarcian–Domerian argillites have been extensively studied at the Tournemire ~~Underground Research Laboratory (~~URL~~)~~, located in a Mesozoic basin on the southern margin of the Massif Central, France (Bonin, 1998). Research at this site, led primarily by the French Institute for Radioprotection and Nuclear Safety (IRSN), focuses on the suitability of these formations for hosting high-level radioactive waste. The sedimentary succession, composed of marlstones and argillites, reaches thicknesses of up to 250 m (Constantin et al., 2004) and was deposited under shallow-marine conditions at estimated water depths of approximately 50 m (Humbezi Desfeux et al., 2024).

Following deposition, compaction and cementation occurred as a result of loading by thick overlying limestone units (Bonin, 1998). 1D thermal history modelling suggests that the formation was buried up to 2,000 m (Barbarand et al., 2001; Peyaud et al., 2005; Mazurek et al., 2006), while other references state depths between 900 - 1,700 m (OECD and NEA, 2022), and 2,500 – 3,000 m during maximum burial (Barbarand et al., 2001; Charpentier et al., 2003). However, the consistently low porosity, typically below 10 % (Boisson et al., 2001; Humbezi Desfeux et al., 2024; Patriarche et al., 2004a), and ~~a~~ predominantly brittle mechanical behaviour that ~~allows for~~results in the formation of ~~fracturing~~ fractures (Constantin et al., 2002; Su et al., 2017) indicates relatively

deep burial. Considering a present day coverage of approximately 300 m (Aalenian to Bathonian lime- and dolostones) (De Windt et al., 1999), and in the absence of directly measured OCR values, the To-Do argillites are estimated to exhibit an OCR of >5, derived from the ratio of reconstructed maximum burial depth to present-day depth under assumed hydrostatic conditions.

Mineralogically, the formation consists of 40–50 wt.% clay minerals, with quartz contributing 10-20 wt.% of the bulk composition. Carbonates (primarily dolomite and calcite), along with pyrite, account for 3-5 wt.% and ~3 wt.%, respectively (De Windt et al., 1999; Boisson et al., 2001). The clay fraction is dominated by illite and kaolinite, with subordinate mixed-layer illite/smectite (with >70 % illite), mica, and minor chlorite (Bonin, 1998; De Windt et al., 1999; Boisson et al., 2001; Constantin et al., 2004).

Hydraulic conductivity data from the Tournemire site are limited and largely derived from Boisson et al. (2001). Hydraulic conductivity values are in the range of 10^{-14} to 10^{-15} m/s from laboratory tests, and 10^{-11} to 10^{-14} m/s from in situ measurements.

2.4 Callovo-Oxfordian Argillite (COx)

The Callovo-Oxfordian argillite, deposited during the Middle Callovian to Middle Oxfordian in the eastern part of the Paris Basin, has been the focus of extensive research over the past three decades. These efforts, led by the French National Radioactive Waste Management Agency (ANDRA), have culminated in the selection of this formation as the host rock for a deep geological repository. Numerous deep boreholes and the Bure Underground ~~Research Laboratory (~~URL~~)~~ are located within a ~250 km² area in the Meuse/Haute-Marne district of north-eastern France (Delay et al., 2007; Distinguin and Lavanchy, 2007; Cosenza et al., 2014).

The COx succession exhibits a consistent thickness exceeding 100 m across the study area and is subdivided into four lithostratigraphic sub-units. These units show a systematic upward trend of decreasing clay content and increasing proportions of silt and carbonates (Gaucher et al., 2004; Cosenza et al., 2014). Mineralogically, the rock is dominated by clay minerals, particularly illite and mixed-layer illite/smectite, with total clay contents reaching up to 60 wt.% (Gaucher et al., 2004; OECD and NEA, 2022).

At present, the top of the formation lies between 400 and 600 m below the surface (Delay et al., 2007). A one-dimensional burial model by Blaise et al.~~,~~ (2014) suggests that the formation experienced maximum burial depths of approximately 850 m (± 200 m) and associated temperatures of around 50 °C during the Late Cretaceous (OECD and NEA, 2022).

~~Hydraulic investigations from b~~Both, laboratory and *in situ* tests consistently report low hydraulic conductivities, typically ranging between 10^{-12} and 10^{-14} m/s (Distinguin and Lavanchy, 2007), supporting the formation's classification as a very low-permeability barrier rock.

Formatiert: Schriftart: Kursiv

2.5 Opalinus Clay Formation (OPA)

The Aalenian (Middle Jurassic) Opalinus Clay Formation, deposited in an epicontinental sea covering large parts of Central Europe, is the designated host rock for high-level radioactive waste disposal in Switzerland (Wetzel et al., 2003; Zimmerli et al., 2024). Over recent decades, extensive research has been conducted on the formation by

numerous institutions and scholars. Under the guidance of the National Cooperative for the Disposal of Radioactive Waste (NAGRA), the Opalinus Clay has been investigated through multiple deep and shallow boreholes across several siting regions in northern Switzerland, as well as in the Mont Terri ~~Underground Research Laboratory (~~URL~~)~~ (Fig.1).

Based on sedimentological features, the OPA is subdivided into three distinct facies zones, characterized by the presence of thin calcareous silty-sand layers or siderite nodules, and a shallowing-upward trend that is reflected in increasing silt and fine sand content toward the top of the formation (Nagra, 2002; Gautschi, 2017; Zimmerli et al., 2024). Mineralogically, the formation is dominated by clay minerals, which make up approximately 59 ± 12 wt.% of the bulk rock composition. Among these, illite is the most abundant (22 ± 8 wt.%), followed by kaolinite (19 ± 6 wt.%), mixed layer illite/smectite ~~mixed layers~~ (14 ± 7 wt.%), and chlorite (7 ± 3 wt.%) (Gautschi, 2017).

The burial history of the OPA is spatially variable. In northern Switzerland, the formation reached maximum burial depths of 1,650–1,700 m, whereas in the Mont Terri area, maximum depths were more modest at around 1,350 m (Mazurek et al., 2006). This burial history is reflected in present-day porosity values, which are generally lower in northern Switzerland (11–12 %) than at Mont Terri (12–18 %) (Gautschi, 2017). Correspondingly, estimated over-consolidation ratios (OCR) based on burial and present-day depth are between 1.5–3 in northern Switzerland and 2.5–5 at Mont Terri (OECD and NEA, 2022).

Hydraulic properties of the OPA have been thoroughly investigated through both laboratory and *in situ* measurements. Reported values ~~for~~ of hydraulic conductivity span a broad range from 10^{-4} to 10^{-14} m/s, depending on location, facies, and depth of the studied rocks (Nagra, 2002; Mazurek et al., 2006; Gautschi, 2017).

In addition to Switzerland, the OPA is also being considered as a potential host rock in Germany, where it is investigated at various locations. Hekel (1994) conducted hydraulic conductivity tests in several shallow wells, demonstrating a clear depth-dependent trend in permeability and influence of local topography. There, the OPA is present a few metre~~s~~ below the surface, representing strongly uplifted rock sections, influenced by decompaction and weathering.

2.6 Boda Claystone Formation (BCF)

The Boda Claystone Formation is the proposed host rock for long-term high-level radioactive waste (HLW) disposal in Hungary (Németh et al., 2016). This Upper Permian unit reaches a thickness of approximately 800–1,000 m and forms part of a much larger, 2,000–4,000 m thick siliciclastic continental sedimentary sequence (Fedor et al., 2008, 2019; Konrád et al., 2010; Németh et al., 2016). Investigations of the BCF began in the 1990s, focusing primarily on several deep boreholes and an underground research laboratory in the Western Mecsek Mountains region. Structurally, the formation is divided into two main blocks: the Boda and Gorica blocks, with most research activities concentrated in the Boda block (OECD and NEA, 2022).

The BCF consists of relatively homogeneous lacustrine sediments deposited in a playa-basin environment, arranged in monotonous sedimentary cycles (Fedor et al., 2008). Lithologically, it can be subdivided into three main units: a lower transitional unit (100–150 m) of fine-grained sandstones, a middle unit (350–450 m) of albite-

rich claystones and siltstones, and an upper unit (400–500 m) of interbedded claystone, albite-rich clayey siltstone, and silty claystone, locally containing dolomite and siltstone beds with desiccation cracks and septarian dolomite concretions (Konrád et al., 2010).

Mineralogically, the BCF is dominated by clay minerals (up to 55 wt.%), primarily illite and chlorite, with minor smectite, kaolinite, and vermiculite. Other significant components include authigenic albite, detrital quartz, carbonate minerals (calcite and dolomite), and hematite (Árkai et al., 2000; Németh et al., 2016).

The BCF experienced substantial burial, reaching maximum depths of approximately 3,500–4,500 m. This which led to extreme consolidation, resulting in over-consolidated (OCR~4.2) highly indurated, brittle rock characterized by very low porosity (mostly <3%) and high bulk densities (~2.6 g/cm³) (OECD and NEA, 2022). Publicly available hydrogeological data for the formation are limited. However, the few available in situ hydraulic test results indicate a wide range of hydraulic conductivities, spanning from 10^{-13} to 10^{-8} m/s. In contrast, laboratory-based water permeability measurements show a much narrower range of K values, consistently between 10^{-13} and 10^{-14} m/s. This large variability suggests a reduced self-sealing effectiveness of fractures, likely related to the high degree of induration and brittle behaviour of the rock (Kovács, 2001).

Table 1 Overview of investigated formations and selected properties. The given data ranges for Boom, To-Do, Cox, and OPA originate from the data compiled in the Clay Club Catalogue of Characteristics of Argillaceous Rocks (CCC) (OECD & NEA, 2022). Data for the AMA originates from Burchartz et al. (2026 5). Given present day depths refer to the formation top at the test location. Porosity ranges are calculated from water content at 105 °C-110 °C. AMA=Amaltheenton Fm, To-Do=Toarcian-Domerian Argillite, COx=Callovo-Oxfordian Argillite, OPA=Opalinus Clay Fm, OCR=over-consolidation ratio, K=hydraulic conductivity, mbgs=metrers below ground surface.

Formation	Thickness (m)	Depth (mbgs)	Max. burial depth (m)	$K_{in\ situ}$ (m/s)	K_{lab} (m/s)	Φ (%)
Boom	102	50-270	205-225	1.6×10^{12}- 8.6×10^{-12}	$4.6 \times 10^{-12*a}$ $9.2 \times 10^{-12*b}$	27.0-44.7
AMA	>90	2-75	1,43300- 3,300	1.2×10^{-7}- 2.7×10^{-5}	1.2×10^{-14}- 3.1×10^{-12}	4.5-15.9
To-Do	200-260	400-560	1,300-1,700	1.0×10^{-15}- 1.0×10^{-13}	$1.0 \times 10^{-14*a}$	7.0-14.0
COx	130-160	400-600	~850 ± 200	1.2×10^{-14}- 3.1×10^{-12}	2.1×10^{-15}- 5.5×10^{-12}	2.6-19.5
OPA	90-160	300-950	1,350-1,700	1.2×10^{-14}- 2.3×10^{-10}	6.0×10^{-15}- 2.0×10^{-13}	5.5-16.2
BCF	210-1,000	0-600	3,500-4,500	1.0×10^{-13}- 8.0×10^{-8}	–	0.5-6.0

*[a] ***best estimate*** perpendicular to bedding*
[b] best estimate parallel to bedding

3 Methods

3.1 Dataset compilation and consolidation

The dataset compiled for this study consists of hydraulic conductivity (K, in m/s) entries, obtained through both laboratory-based and *in situ* testing across six argillaceous formations in Europe (Fig. 1). Primary data sources include peer-reviewed publications, technical reports, and theses, and were supplemented with data ranges from the Clay Club Catalogue (OECD and NEA, 2022). A complete reference list is given in Table A1.

Most data were collected from vertical boreholes, either drilled from the surface or accessed via ~~underground research laboratories (~~URL`s~~)~~. In a few cases, *in situ* data were derived from horizontal boreholes. Where reported, borehole and sample orientation relative to bedding or stratification was considered, allowing for an assessment of hydraulic anisotropy.

To ensure the comparability and consistency of the dataset, a set of inclusion criteria was applied during data selection. These include:

i. A credible and well-documented testing methodology (laboratory or *in situ*).
ii. A clearly defined spatial location and depth, allowing for stratigraphic correlation.
iii. Overlap or close proximity between lab and *in situ* data, minimizing the risk of significant sedimentological or diagenetic variability.
iv. Availability of information on the maximum depth experienced during burial diagenesis.
v. Presence of mineralogical data, either for tested samples, borehole sections, or nearby stratigraphic equivalents.

In addition to hydraulic conductivity data, petrophysical parameters such as porosity, grain density, and bulk density were included to support the interpretation of burial- and diagenesis-related trends. Porosity values were derived from standard petrophysical methods, including gravimetric water-loss after drying at 105 °C, bulk-density/grain-density relationships, and helium pycnometry. Accordingly, these values represent matrix properties of intact samples and do not account for fracture porosity. Similarly, laboratory hydraulic conductivity measurements represent matrix hydraulic conductivity, whereas field-scale measurements were retained as reported in the original sources and may reflect bulk rock-mass behaviour where fractures or other heterogeneities are present.

3.2 Test methods to evaluate hydraulic conductivity

The hydraulic conductivities compiled for this study were based on various test methods and types. The abundance of each test method across the dataset and individual formations is shown in Fig. 2. It is recognizable that the vast majority of laboratory-based hydraulic conductivities is derived by permeameter tests (e.g.~~i.e.~~ flow-through tests), while *in situ* methods are dominated by packer tests. Laboratory experiments were predominantly conducted on intact core plugs and are therefore considered representative of matrix hydraulic properties. In contrast, *in situ* measurements may incorporate the hydraulic influence of fractures and other rock-mass heterogeneities and are therefore interpreted as bulk rock-mass hydraulic conductivity.~~.~~

Formatiert: Schriftart: Kursiv

Here, only a concise overview is given of the different testing methods in Tables 2 and 3. For detailed information, the reader is referred to the references given in the tables.

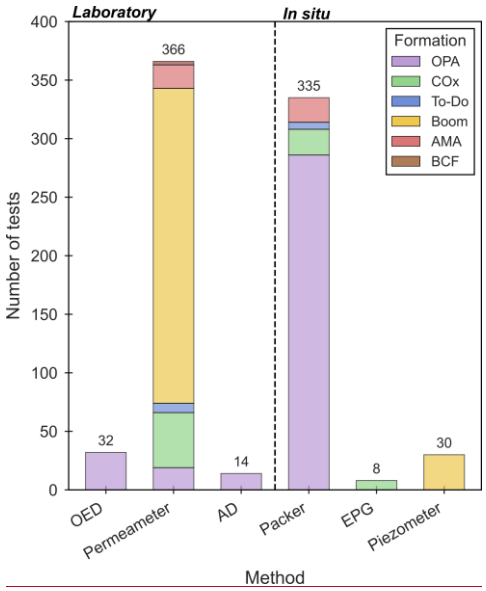
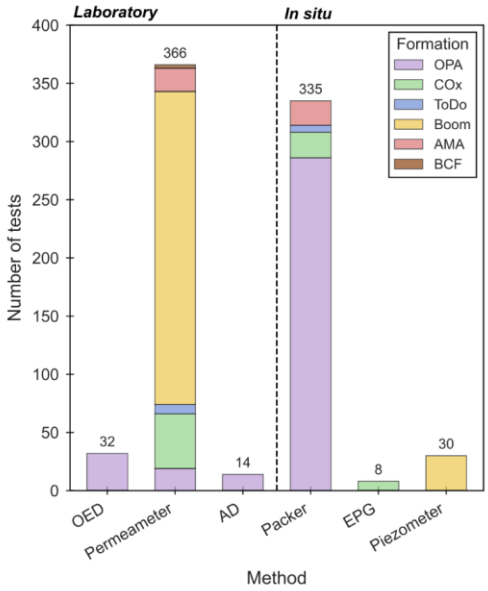


Figure 2 Distribution of hydraulic conductivity test methods used across all investigated formations. Bars show the total number of laboratory (left of dashed line) and in situ (right of dashed line) measurements, subdivided by formation. Numbers above the bars indicate the total count per method. OED=Oedometric tests, AD=Advective displacement tests, Packer=Packer tests, EPG=Electromagnetic pressure gauge.



~~*Figure 2 Distribution of hydraulic conductivity test methods used across all investigated formations. Bars show the total number of laboratory (left of dashed line) and in situ (right of dashed line) measurements, subdivided by formation. Numbers*~~

Formatiert: Nicht vom nächsten Absatz trennen

Formatiert: Beschriftung, Abstand Nach: 0 Pt., Rahmen: Oben: (Kein Rahmen), Unten: (Kein Rahmen), Links: (Kein Rahmen), Rechts: (Kein Rahmen)

~~above the bars indicate the total count per method. OED=Oedometric tests, AD=Advective displacement tests, Packer=Packer tests, EPG=Electromagnetic pressure gauge.~~

Table 2 Overview of laboratory-based methods for the estimation of hydraulic conductivity (K).

Method	Basic Principle	References
Oedometer (OED)	Axially loaded specimen in a rigid ring; infers K from extended consolidation theory during loading by relating it to the coefficient of volume change and compressibility at each state of consolidation (indirect measurement of K)	~~(Aertsens et al., 2004, 2008, 2013;~~ Batlle-Aguilar et al., (2016); Ferrari et al., (2016); Favero, (2017); Crisci et al., (2019); Ferris et al., (2020)
Permeameter	Constant-head or ~~pulsed fluid flow through~~pressure pulse decay on ~~saturated~~ core plug samples; K is derived from Darcy's law	(Aertsens et al., (2003, 2004, 2013; Fedor et al., (2008); Wemaere et al., (2008); Yu et al., (2013, 2017); Favero et al., (2018); Giger et al., (2018)
Advective displacement (AD)	Advective displacement of *in situ* pore water with artificial pore fluid under large hydraulic gradients; K inferred from sample dimensions and average volumetric flow rate over time	Mäder, (2018); Nagra, (2020); Kiczka et al., (2023)

Table 3 Overview of in situ methods for the estimation of hydraulic conductivity (K).

Method	Basic Principle	References
Packer Test	Isolates borehole section; injects/extracts water; measures pressure/flow over time to infer K, applied tests comprise pulse, slug or constant rate tests	(Bredehoeft and Papadopulos, (1980); Boisson et al., (2001); Distinguin and Lavanchy, (2007); Nagra work reports Dossier VII (e.g. Wersin et al., 2022)
Piezometer	Monitors hydraulic head at discrete depths; K from recovery or long-term pressure response	Bastiaens et al., (2007); L. Yu et al., (2013) and references therein
Electro-magnetic Pressure Gauge (EPG)	Long-term, isolated pressure monitoring; K inferred from pressure over time recovery trends	Distinguin & Lavanchy, (2007)

3.3 Data discretisation and analysis

3.3.1 Natural variability of hydraulic conductivity

The compiled dataset originates from a range of laboratory and *in situ* techniques and various investigation sites. This inherently introduces biases into the results, arising from methodological factors (e.g., scale effects, effective stress conditions during laboratory tests) and natural factors due to intrinsic heterogeneity (e.g., compositional variability among stratigraphic subunits or sampling sites, bedding anisotropy), all of which contribute to natural scatter in the hydraulic data (Neuzil, 1994), even within the same formation. Available information on both methodological and geological controls was systematically assessed, with particular focus on parameters that could be consistently quantified across data sources. For methodological aspects, this included:

1. The distinction between field and laboratory datasets,
2. The interval length of *in situ* tests, and

Formatiert: Deutsch (Deutschland)
Formatiert: Deutsch (Deutschland)
Feldfunktion geändert
Formatiert: Deutsch (Deutschland)
Formatiert: Deutsch (Deutschland)
Formatiert: Deutsch (Deutschland)
Formatiert: Deutsch (Deutschland)
Formatiert: Deutsch (Deutschland)
Formatiert: Deutsch (Deutschland)
Formatiert: Deutsch (Deutschland)
Formatiert: Deutsch (Deutschland)
Formatiert: Deutsch (Deutschland)

3. The applied effective confining stress during laboratory experiments.

Where reported, sample orientation with respect to the bedding was ~~accounted~~ considered to assess the anisotropy across the laboratory-derived data.

The resulting scatter in the hydraulic conductivity data, for tests conducted under comparable boundary conditions, is here referred to as natural variability. This baseline serves as a reference framework for subsequent analyses. Observations that fall within the observed variability envelope are interpreted as expected scatter related to geological heterogeneity and methodological factors. In contrast, values that deviate substantially from this baseline are considered to reflect geological or mechanical processes beyond natural variability, such as fracture-dominated flow. As a simple measure to consolidate this natural variability, we report the interquartile range (IQR, the difference between the 75th and 25th percentiles of $\log_{10}K$) for laboratory and *in situ* data from the diagenetically consolidated formations (excluding Boom Clay and data affected by near-surface effects such as decompaction or weathering).

Formatiert: Schriftart: Kursiv

In order to observe formation specific scale contrasts between laboratory- and field-derived hydraulic conductivities, the data was discretized in ~~10~~ 40 m depth bins. For each bin, the geometric mean and median were calculated. Subsequently, the offset ($\Delta log_{10}K$) between *in situ* and laboratory K was computed as:

$$\Delta log_{10}(K) = log_{10}K_{in\ situ} - log_{10}K_{lab} \quad (2\text{~~1~~})$$

This approach quantifies systematic shifts between the sub-datasets and allows investigation of how these shifts vary with depth. The BCF is excluded as no discrete *in situ* data is accessible for this formation from literature.

3.3.2 ~~*Burial estimates*~~*Maximum burial depth estimations*

The evolution of hydraulic conductivity along the formations' burial history is a central part of the present study. The compiled dataset contains data from six formations, sampled across various investigation sites, and a present-day depth range of a few metres to approximately 1,100 m below ground level. This strong variability ~~promotes the fact, that~~arises because detailed data for burial reconstruction are not available for each test site and depth. However, general burial trends can be found for all formations, mostly derived from basin modelling or indicators of maximum heating such as apatite fission-track and vitrinite reflectance. Hence, the analysis of burial history-related alterations of hydraulic conductivity is limited to data ranges. The burial parameters, underlying methods, and respective references considered here are summarized in Table 4.

The ~~Opalinus Clay~~OPA and COx burial reconstructions are~~is~~ based on 1D basin modelling ~~carried out by Mazurek et al. (2006)~~ (Mazurek et al., 2006; Blaise et al., 2014). For OPA, t~~T~~he given burial depths and peak ~~burial~~ temperatures reached during maximum burial (T_{peak}) refer to the locations of boreholes Rinken, Weiach, and Benken, and the Mont Terri URL. The hydraulic conductivity data derived from other locations of OPA were assigned to these sites and burial characteristics with respect to their affiliation with the siting regions in northern Switzerland: Jura Ost (JO), Nördlich Lägern (NL), and Zürich Nordost (ZNO). Shallow OPA data from boreholes in the Swabian Alb (Germany), and the Lausen borehole (Switzerland) lack detailed maximum burial depth estimates. For To-Do and BCF T_{peak} and associated maximum burial depths are derived from vitrinite reflectance

Formatiert: Tiefgestellt

and phyllosilicate crystallinity. Detailed and recent burial reconstruction from 3D basin modelling is available for the AMA from five borehole locations (BO1 – BO5) in the SE margin of the Lower Saxony Basin (Castro-Vera et al., 2024).

Table 4 Summary of estimated maximum burial depths for the investigated argillaceous formations, including site-specific information where available. Burial depth estimates are based on regional burial history reconstructions and borehole-specific studies. References indicate the primary sources for each estimate. T_{peak}=~~maximum~~ peak ~~temperature reached along burial history~~burial temperature.

Formation	Sub region/borehole	Max. burial depth (m)	T_{peak} (°C)	Method	Reference
OPA	Mont Terri URL (MT) Rinken (Jura Ost) Weiach (Nördlich Lägern) Benken (Zürich Nordost)	1,350 1,550 1,700 1,650	85 - 84 85	1D Thermal basin modelling	Mazurek et al., (2006); Nagra, (2002)
COx	Meuse-Haute-Marne URL and adjacent boreholes	850	50	1D Thermal basin modelling	Blaise et al., (2014); OECD and NEA (2022)
To-Do	Tournemire	2,000	≥110	Appatite fission-track, Rock-Eval pyrolysis, fluid inclusions	(Barbarand et al., (2001); Peyaud et al., (2005); Mazurek et al., (2008, 2011)
AMA	BO1 BO2 BO3 BO4 BO5	1,550 1,400 2,100 2,440 3,300	93 83 116 127 163	3D Thermal basin modelling	(Castro-Vera et al., (2024; Burchartz et al., (2026)
Boom*[a]	Doel-2b Zoersel Essen-1 Mol-1 Weelde-1	58 89*[b] 159*[b] 191*[b] 260*[b]			Mertens et al., (2003); Wemaere et al., (2008)
BCF	Western Mecsek Mountains	3,500-4,500	200-250	Vitrinite reflectance and phyllosilicate crystallinity	(Árkai et al., (2000); OECD and NEA, (2022) and references therein

[a] given depths refer to formation top
[b] top of transition zone

Formatierte Tabelle

4 Results

The compiled dataset consists of 782 entries for hydraulic conductivity, of which 370 entries stem from *in situ* measurements. and 412 values ~~were derived~~ from different laboratory methods. Additionally, petrophysical and mineralogical data were gathered for all investigated formations and are represented by 292 entries of porosity, 141 entries of grain density, 115 entries of bulk density, and data for bulk mineralogical composition, summarizing clay mineral content, carbonate content, and amount of quartz + feldspars + accessories.

4.1 Hydraulic conductivity distribution

The compiled dataset of 782 hydraulic conductivity (K) measurements span twelve orders of magnitude, from 10^{-16} to 10^{-4} m/s (Fig. 3) and covers a depth range of few metreers below surface and approximately 1,100 m (Fig. 4). *In situ* test results (n = 370) display substantially greater scatter in hydraulic conductivity than laboratory data, and

range between 10^{-15} to 10^{-4} m/s as opposed to laboratory data which range between 10^{-16} to 10^{-10} m/s). Formation-specific K distributions and selected summary statistics are given in Table 5.

The Opalinus Clay Formation exhibits the broadest variability in hydraulic conductivity and depth range, with *in situ* values extending from 10^{-14} to 10^{-4} m/s (n = 284), depending on test depth that covers tests from a shallow zone (0 - 65 m) and an intermediate to deep zone (250 – 1,065 m). Laboratory results show a significantly lower spread and cluster between 10^{-14} and 10^{-12} m/s. Effective stress conditions applied during test performance lie between 5 —and 50 MPa. The Boom Clay dataset includes 269 laboratory measurements, primarily from permeameter and migration experiments, giving K values from 10^{-13} to 10^{-10} m/s. The lab ssamples stem from five boreholes in northern Belgium and cover a depth range between 59 and 366 m. *In situ* data from piezometer pressure-recovery tests (n = 30) fall within a narrower range between 10^{-12} and 10^{-11} m/s, derived from boreholes drilled from the HADES URL in Mol with test depths between 223 – 258 m. The Callovo–Oxfordian argillite, represented by 81 hydraulic conductivity entries from the Bure URL and boreholes in close proximity, shows close agreement between laboratory measurements (10^{-16} to 10^{-12} m/s) and *in situ* tests (10^{-15} to 10^{-12} m/s). Sample depths for laboratory tests range between 353 - 543 m, while in situ tests were carried out between 355 – 630 m depth. The Toarcian–Domerian argillite (To-Do) is represented by a modest dataset derived from the Tournemire URL, with laboratory K values between 10^{-14} and 10^{-13} m/s (n = 8; sample depths between 230 - 339 m) and in situ results spanning from 10^{-14} to 10^{-11} m/s (n = 6; test depths between 275 - 380 m). The Amaltheenton Formation displays a pronounced lab–field contrast, with laboratory values of 10^{-14} to 10^{-12} m/s and *in situ* results several orders of magnitude higher, ranging from 10^{-11} to 10^{-5} m/s. This formation was investigated based on several shallow boreholes (<100 m depth) in the eastern margin area of the Lower Saxony Basin, Germany (Gaus et al., 2022; Castro-Vera et al., 2024; Burchartz et al., 2026). The Boda Claystone Formation is represented by a small number of water permeability measurement results that lie between $1.1x10^{-14}$ and $1.3x10^{-13}$ m/s. Samples originate from depths around 1,000 m, taken from boreholes drilled from the Alpha shaft URL (Fedor et al., 2008). *In situ* data of the BCF is sparse. For this study the data range given in the CCC (OECD and NEA, 2022) was adapted. It shows hydraulic conductivities in a wide scatter between 10^{-13} and 10^{-8} m/s. A given and a best estimate is atof $1.0 \times x10^{-12}$ m/s. The meaning of "best estimate" for the BCF is not further differentiated in the CCC. However, but it generally serves reference valueas selected or calculated reference value based on expertise from the available data (OECD and NEA, 2022).

Table 5 Selected hydraulic conductivity (K) summary statistics by formation and method, reporting sample size (n), min, max, geometric mean, and standard deviation. OPA=Opalinus clay, Cox=Callovo-Oxfordian argillite, To-Do=Domerian-Toarcian argillite, AMA=Amaltheenton Fm., mbgs=meters below ground surface, Geom.=Geometric.

Formation	Method	n	Depth range (mbgs)	K_{Min} (m/s)	K_{Max} (m/s)	Geom. Mean (m/s)	Std. Dev. ($log_{10}K$)
OPA	Lab	65	464-987	$1.00 \times x10^{-14}$	$1.20 \times x10^{-12}$	$1.18 \times x10^{-13}$	0.45
	In Situ	284	4-908	$1.00 \times x10^{-14}$	$8.00 \times x10^{-4}$	$2.29 \times x10^{-9}$	2.75
COx	Lab	47	353-542	$8.27 \times x10^{-16}$	$1.05 \times x10^{-12}$	$6.31 \times x10^{-14}$	0.65
	In Situ	30	355-630	$9.00 \times x10^{-15}$	$1.10 \times x10^{-12}$	$1.59 \times x10^{-13}$	0.56
To-Do	Lab	8	230-339	$1.00 \times x10^{-14}$	$1.20 \times x10^{-13}$	$3.80 \times x10^{-14}$	0.44
	In Situ	6	276-394	$1.40 \times x10^{-14}$	$2.30 \times x10^{-11}$	$3.92 \times x10^{-13}$	1.16
Boom	Lab	269	59-365	$2.10 \times x10^{-13}$	$3.51 \times x10^{-10}$	$4.65 \times x10^{-12}$	0.43

Formation	Method	n	Depth range (mbgs)	K_{Min} (m/s)	K_{Max} (m/s)	Geom. Mean (m/s)	Std. Dev. ($log_{10}K$)
	In Situ	30	223-256	2.60×10^{-12}	1.70×10^{-11}	4.53×10^{-12}	0.16
AMA	Lab	20	58-98	1.47×10^{-14}	2.15×10^{-12}	1.99×10^{-13}	0.58
	In Situ	20	54-95	7.62×10^{-11}	3.43×10^{-5}	4.58×10^{-8}	1.68
BCF	Lab	3	~1,000	1.1×10^{-14}	1.3×10^{-13}	4.50×10^{-14}	0.40
	In Situ*[a]		330-830	2.0×10^{-13}	8.0×10^{-8}	1.0×10^{-12}	

*[a] *data range taken from the CCC* OECD & NEA, (2022)

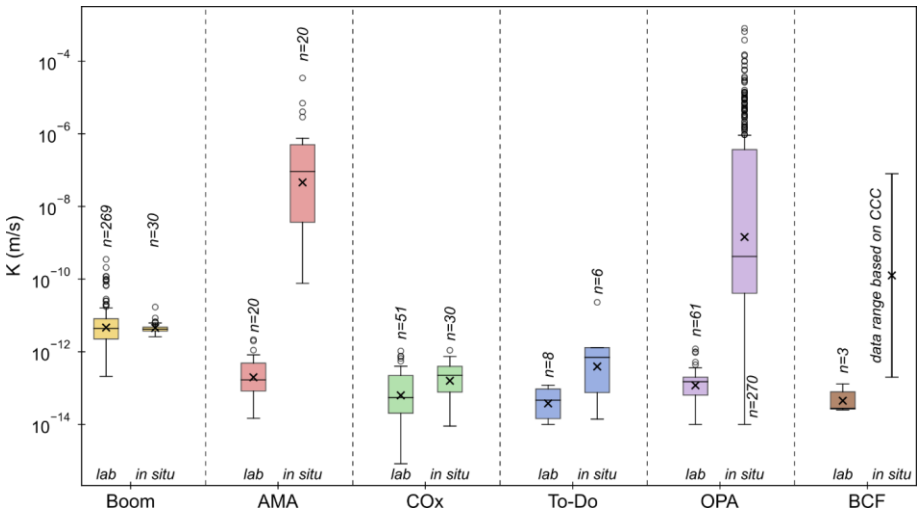


Figure 3 Hydraulic conductivity boxplots from laboratory and in situ measurements by formation. Boxes represent interquartile range (25th–75th percentile), horizontal lines indicate the median, and the x-marker the geometric mean. Whiskers span the 10th–90th percentile. Individual points represent outliers. CCC=Clay Club Catalogue OECD & NEA, (2022).

4.2 Present-day depth trend

The compiled hydraulic conductivities span a depth range from near-surface (a few metreers below ground) to ~1,100 m true vertical depth. Most *in situ* tests (n = 242) are concentrated at depths shallower than 100 m, while laboratory samples predominantly originate from deeper intervals (Fig. 4). Overall, the *in situ* ~~data~~ hydraulic conductivity shows a pronounced decrease ~~in hydraulic conductivity~~ within the ~~upper~~ first 100 m of present-day depth, spanning~~of~~ nine orders of magnitude (10^{-13} to 10^{-4} m/s)~~.~~, ~~while~~ In contrast, laboratory data from the AMA and OPA from the same depth lie in a distinctively narrower range between 10^{-14} to 10^{-12} m/s. ~~Tests on AMA samples were conducted at effective stresses between 1 and 20 MPa, whereas OPA samples from Lausen were tested under effective stress conditions ranging from 0 to 50 MPa.~~ Between ~200 m and ~1,100 m, laboratory and field-derived K of over-consolidated, lithified formations (OPA, COx, To-Do) converge and predominantly show clustering within a range of 10^{-14}~~^{2}~~ to 10^{-12}~~^{4}~~ m/s. An exception to this is the BCF, where *in situ* values show a significantly wider scatter with hydraulic conductivities up to 10^{-8} m/s, while lab values fall between 10^{-14}~~^{3}~~ and 10^{-13}~~^{4}~~ m/s. The ~~less~~ slightly over-consolidated Boom Clay shows a minor monotonic depth trend and a generally low scatter over a depth range of 59 to 366 m. Field and laboratory data between 223 and 260 m overlap closely,

spanning from 10^{-12} to 10^{-11} m/s. Across the moderately to strongly over-consolidated formations (OPA, COx, To-Do, BCF), the central 50 % of data at present-day depths >100 m fall within an interquartile range of 3.9×10^{-14} to 2.4×10^{-13} m/s (*in situ*) and 3.3×10^{-14} to 2.3×10^{-13} m/s (laboratory), corresponding to a factor of ~6–7 in both cases, i.e., less than one order of magnitude, and in close agreement between the two datasets.

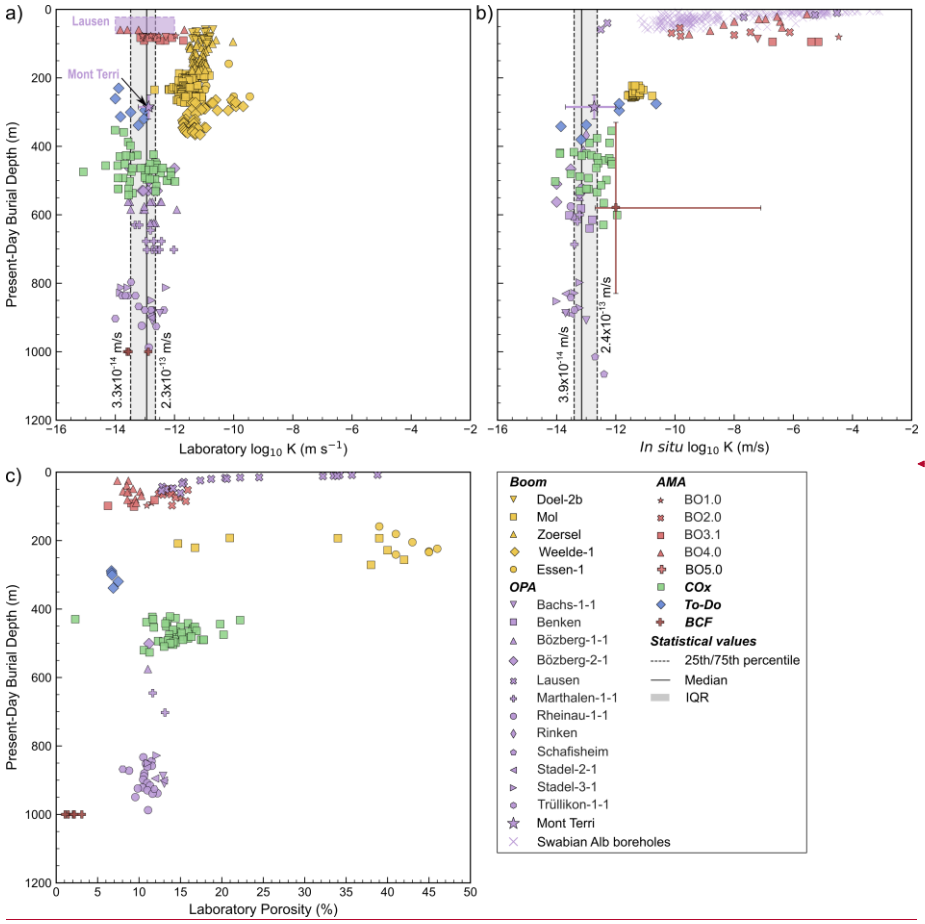
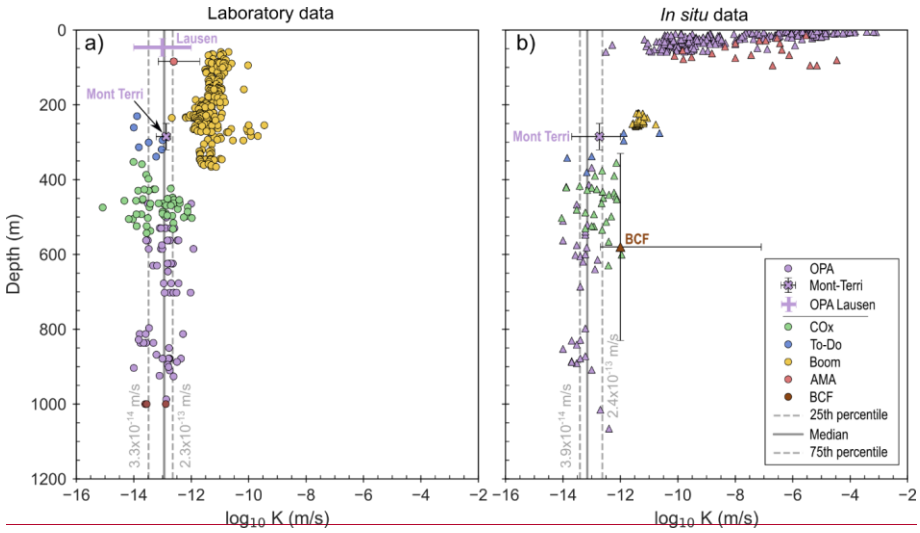


Figure 4 Log hydraulic conductivity (K) over depth plot of a) laboratory derived K; b) in situ experiment derived K, divided by formation. The plotted interquartile range (IQR) represent the data of moderately to strongly over-consolidated argillaceous rock formations (OPA, COx, To-Do, BCF) filtered for depths >100 m. This filter was applied to minimize the influence of near-surface decompaction and weathering, which might dominate hydraulic variability in the shallowest interval. The in situ data for the BCF represents the data range given by the CCC (OECD and NEA, 2022); c) porosity versus present-day burial depth distribution of the compiled data-set.

Formatiert: Hochgestellt
Formatiert: Hochgestellt
Formatiert: Schriftart: Kursiv
Formatiert: Hochgestellt
Formatiert: Hochgestellt
Formatiert: Nicht vom nächsten Absatz trennen
Formatiert: Beschriftung, Abstand Nach: 0 Pt., Rahmen: Oben: (Kein Rahmen), Unten: (Kein Rahmen), Links: (Kein Rahmen), Rechts: (Kein Rahmen)



~~*Figure 4 Log hydraulic conductivity (K) over depth plot of a) laboratory derived K, b) in situ experiment derived K, divided by formation. The plotted interquartile ratios represent the data of moderately to strongly overconsolidated argillaceous rock formations (OPA, COx, To-Do, BCF) filtered for depths >100 m. The in situ data of the BCF represents the data range given by the CCC (OECD and NEA, 2022).*~~

4.3 Factors controlling natural variability of hydraulic conductivity

4.3.1 Measurement scale

The compiled *in situ* dataset spans a broad range of packer test interval lengths, from <1 m to over 120 m (Fig. 5). Most tests were performed over intervals shorter than 40 m, while only a few exceed 100 m. For the OPA, COx, and To-Do formations, hydraulic conductivities derived from packer tests fall consistently within a narrow range of 10^{-12} to 10^{-14} m/s, regardless of interval length. Notably, 50 % of these data at present-day depths >100 m cluster even more tightly, within a interquartile range of 0.79 $\log_{10}$ units (between $3.9 \times$ ~~×~~10^{-14} and $2.4 \times$ ~~×~~10^{-13} m/s) (~~interquartile range,~~ Fig. 5a). Within this depth range, no systematic effect of interval length is apparent.

Formatiert: Tiefgestellt

In contrast, packer tests performed at depths <100 m provide a more complex picture. These data originate exclusively from the OPA and AMA. For the OPA, interval lengths are reported in detail for tests from the Lausen borehole, ranging from ~4 m to ~23 m (Vogt et al., 2017). Interestingly, hydraulic conductivities derived from the longer intervals (14 m and ~23 m) are several orders of magnitude lower than those from shorter intervals (4 – 9 m), with values around 10^{-13} m/s compared to 10^{-8} to 10^{-5} m/s, respectively. This difference, however, coincides with depth: the longer intervals are located exclusively below ~30 m, outside the decompaction-influenced zone identified by Vogt et al. (2017). OPA data from shallow boreholes in the Swabian Alb (Germany) are not included in Fig. 5, as interval lengths for the corresponding packer tests are not reported in the source literature~~do not include continuous reports of interval lengths~~ (Hekel, 1994).

The AMA was investigated in four boreholes, with most packer tests performed on short intervals of <10 m, and some longer ones of up to 84 m (BO4.0). No systematic scale-dependence is observed in the shorter intervals.

~~However, two clear interval length-related trends appear in BO2.0 and BO4.0: in the latter,~~ In BO4.0 K decreases by three orders of magnitude (down to 3 × ~~x~~10^{-10} m/s) in ~~the deeper~~test intervals located at depths ~~borehole sections between~~ of 45 – 95 m. However, as these longer intervals coincide with greater present-day depth (similar to the Lausen data discussed above), the limited number of measurements (n=3) does not allow us to robustly disentangle a possible interval-length effect from the depth-dependent trend.

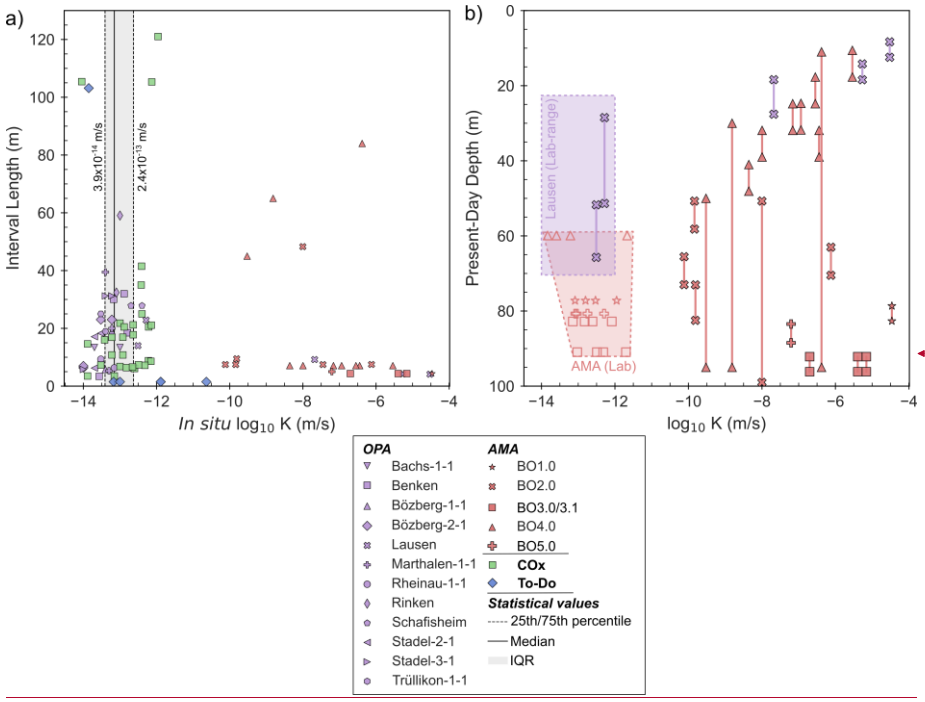
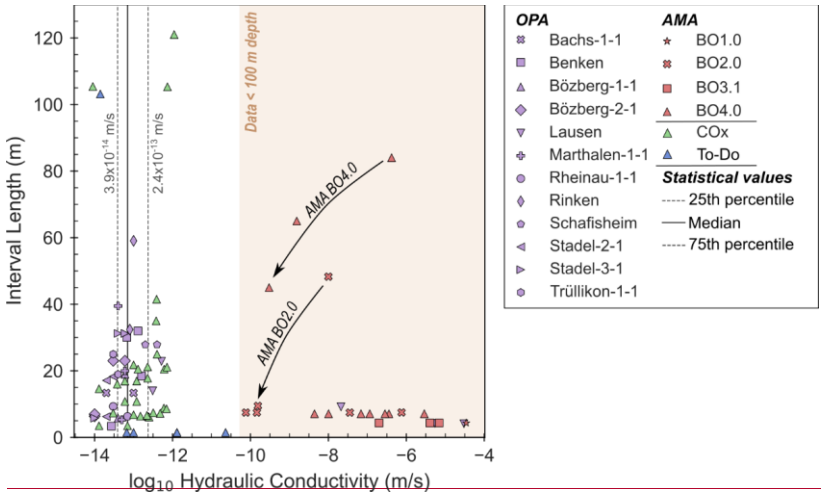


Figure 5 a) Relationship between packer interval length and hydraulic conductivity from in situ packer tests. The dashed vertical lines represent the 25 and 75 percentiles and the grey box the IQR of data from depth >100 m. ~~Arrows indicate the pronounced decrease of K with decreasing interval length observed in the AMA boreholes BO2.0 and BO4.0~~. The BCF is excluded as no discrete in situ data is accessible for this formation from literature; b) present-day depth versus log_{10}K plot of the uppermost 100 m present-day depth with lab ranges and packer test results from the Lausen borehole (OPA; lab range after Crisci et al. 2019, in situ data after Vogt et al. 2017) and packer test and lab test results from several AMA boreholes. The vertical lines represent the test intervals from packer tests, with borehole-specific markers placed at the upper and lower end.~~

Formatiert: Nicht vom nächsten Absatz trennen

Formatiert: Beschriftung, Abstand Vor: 0 Pt., Nach: 0 Pt.

Formatiert: Tiefgestellt



~~Figure 5 Relationship between packer interval length and hydraulic conductivity from in situ packer tests. The dashed vertical lines represent the IQR of data from depth >100 m. Arrows indicate the pronounced decrease of K with decreasing interval length observed in the AMA boreholes BO2.0 and BO4.0. The BCF is excluded as no discrete in situ data is accessible for this formation from literature.~~

A direct comparison between laboratory and *in situ* results was made using the computed offset $\Delta\log_{10}K$ between median and geometric mean values (Fig. 6). ~~In~~ For the AMA, this offset is large, with $\Delta\log_{10}K$ values exceeding 6, highlighting a strong lab–field contrast at shallow depths. Similarly, data from the Lausen borehole at depths <30 m indicate a similar divergence. These results are not included in Fig. 6, as only the range of laboratory-derived hydraulic conductivities is publicly available (Crisci et al., 2019). For laboratory K, derived from oedometric and constant-head permeameter experiments conducted on samples from depths between ~23~~20~~ and ~70 m ~~depth~~, hydraulic conductivities consistently fall within 10^{-14} to 10^{-12} m/s, depending on the applied effective ~~confining~~ stress during tests. In contrast, *in situ* measurements from <30 m depth yield much higher values, between 10^{-8} and 10^{-5} m/s (Fig. 5b). This discrepancy corresponds to hypothetical $\Delta\log_{10}K$ values of 4 to 8, similar to those observed for the AMA. However, this contrast disappears in the Lausen borehole at depths >30 m, where hydraulic conductivities from *in situ* and laboratory experiments converge and overlap (Crisci et al., 2019). In contrast, for the AMA, laboratory-derived K values consistently remain below the corresponding *in situ* measurements.

By comparison, for Boom, OPA, COx, and To-Do (all sampled at depths >200 m), the offset is much smaller, within 1 – 2 orders of magnitude. This indicates close agreement between laboratory- and field-derived conductivities at greater depths and across different investigation scales. For indurated, lithified formations (OPA, COx, To-Do), the ~~interquartile ratios~~IQR below 200 m depth further indicate very little scatter between the lab and field scale (Fig. 6). Moreover, the IQR~~interquartile ratios~~ of laboratory and *in situ* data from the indurated, over-consolidated formations at depths below 1~~2~~00 m (grey numbers in Fig. 4) are in close agreement. For the BCF, a direct calculation of $\Delta\log_{10}K$ could not be performed, as only data ranges for *in situ* measurements are

Formatiert: Standard, Abstand Vor: Automatisch, Nach: Automatisch, Nicht vom nächsten Absatz

Formatiert: Abstand Vor: 0 Pt., Nach: 0 Pt.

available, and there is no depth overlap between laboratory and field hydraulic conductivities. However, a clear contrast emerges from the available data (see Fig. 4~~):~~) in that field-based measurements at depths between 400 and 800 m report hydraulic conductivity values as high as 10^{-8} m/s, whereas laboratory experiments consistently yield much lower values, in the range of 10^{-14} to 10^{-13} m/s.

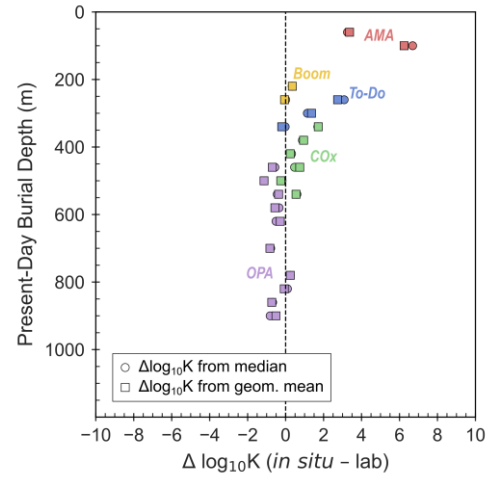
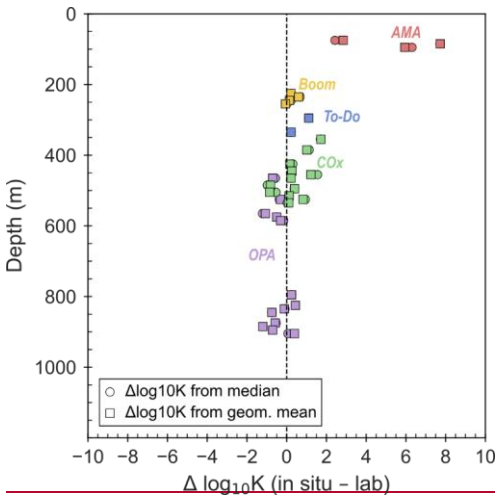


Figure 6 Depth-binned (40 m bins) comparison of laboratory and in situ hydraulic conductivity measurements for individual formations. The BCF is excluded as no discrete in situ data is accessible for this formation from literature.

Formatiert: Beschriftung, Abstand Vor: 0 Pt., Nach: 0 Pt.

Formatiert: Englisch (Vereinigtes Königreich)



~~*Figure 6 Depth-binned (10 m bins) comparison of laboratory and in situ hydraulic conductivity measurements for individual formations. The BCF is excluded as no discrete in situ data is accessible for this formation from literature.*~~

4.3.2 Hydraulic anisotropy

Laboratory measurements for which the flow direction with respect to bedding orientation was reported (n=3637) were separated into tests performed parallel (K_P; n=1345) and perpendicular (K_S; n=22932) to bedding, with the Boom Clay representing 64 % of all datapoints with 92 K_p and 141 K_s values. No bedding orientations are reported for measurements done on To-Do and BCF samples. Hydraulic conductivities for both orientations span over four orders of magnitude Within the remaining formations, geometric means indicate a systematic, though variable, shift towards higher values parallel to bedding, but distributions show a slight systematic shift towards higher values in the parallel direction (Table 6 and Fig. 7). The anisotropy ratio (K_P/K_S) ranges from 1.07 (OPA) and 1.23 (COx), indicating near-isotropic behaviour, to 1.55 (AMA) and 2.72 (Boom), the latter showing the most pronounced anisotropy among the investigated formations. Parallel tests yield a geometric mean of $2.4x10^{-12}$ m/s, approximately three times higher than in the perpendicular direction ($8.3x10^{-13}$ m/s). Median values show a similar relationship with $5.2x10^{-12}$ m/s versus $1.6x10^{-12}$ m/s, respectively. The partly subtle but observed K_P-K_S contrast in the global datasets can be attributed to the intrinsic anisotropy of the argillaceous nature of investigated formations.

Table 6 Sample size (n) and geometric mean hydraulic conductivity parallel (K_p) and perpendicular (K_s) to bedding, by formation, with the resulting anisotropy ratio (K_p/K_s). To-Do and BCF lacked reported bedding orientation and are excluded.

Formation	n (K_p/K_s)	Geom. Mean K_p (m/s)	Geom. Mean K_s (m/s)	K_p/K_s
Boom	92/141	9.53×10^{-12}	3.51×10^{-12}	2.72
COx	12/35	7.91×10^{-14}	6.45×10^{-14}	1.23
OPA	22/41	1.23×10^{-13}	1.15×10^{-13}	1.07
AMA	8/12	2.59×10^{-13}	1.67×10^{-13}	1.55

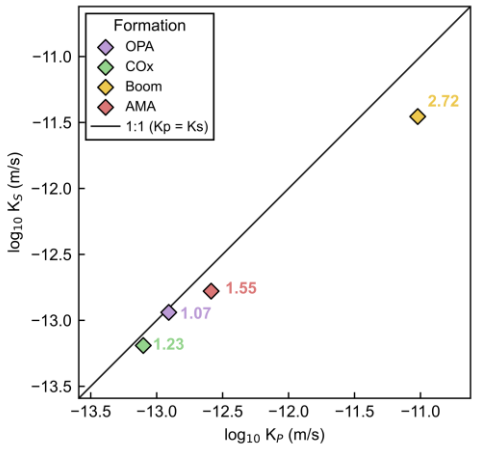
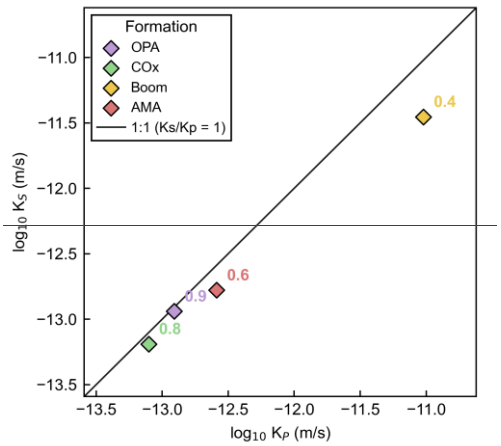


Figure 7 Log_{10} hydraulic conductivity perpendicular to bedding (K_s) versus parallel to bedding (K_p) for the investigated formations. Symbols show geometric mean values. The solid line marks isotropic conditions (K_p/K_s = 1). Numbers denote anisotropy ratios (K_p/K_s), showing slightly lower hydraulic conductivity perpendicular to bedding in all cases.

Formatiert: Tiefgestellt
Formatiert: Tiefgestellt
Formatiert: Tiefgestellt
Formatiert: Tiefgestellt
Formatiert: Beschriftung, Nicht vom nächsten Absatz trennen
Formatiert: Tiefgestellt
Formatiert: Tiefgestellt
Formatiert: Zeilenabstand: einfach
Formatiert: Zeilenabstand: einfach
Formatiert: Zeilenabstand: einfach
Formatiert: Zeilenabstand: einfach
Formatiert: Zeilenabstand: einfach
Formatiert: Nicht vom nächsten Absatz trennen
Formatiert: Beschriftung, Abstand Vor: 0 Pt.
Formatiert: Tiefgestellt
Formatiert: Tiefgestellt
Formatiert: Tiefgestellt
Formatiert: Tiefgestellt



~~*Figure 7 Log$_{10}$ hydraulic conductivity perpendicular to bedding (K_s) versus parallel to bedding (K_p) for the investigated formations. Symbols show geometric mean values. The solid line marks isotropic conditions (K_s/K_p = 1). Numbers denote anisotropy ratios (K_s/K_p), showing slightly lower hydraulic conductivity perpendicular to bedding in all cases.*~~

4.3.3 Stress dependency of laboratory data

Where available, effective ~~confining~~ stresses conditions applied during ~~permeameter~~ laboratoy experiments were incorporated into the compiled dataset. The type of applied effective stress differs depending on formation and test-type: for OPA, hydraulic conductivity was predominantly derived from oedometer consolidation theory on samples from various boreholes, supplemented by constant-head permeability tests performed on a subset of samples at defined stages of applied vertical effective stress (σ'_v), ranging from 5 to 15 MPa (Fig. 8a). For AMA, values represent effective confining stress (σ'_c) applied during water-saturated constant-head testing, varied systematically between 1 and 20 MPa (Fig. 8b). In contrast, BCF and To-Do, effective confining stress during pressure pulse-decay testing was held quasi-constant (6.4 – 7.0 MPa and 3 MPa, respectively) rather than systematically varied.

Figure 8 shows hydraulic conductivity plotted against the respective effective stress. For OPA, all data points cluster within two orders of magnitude (10^{-14} to 10^{-12} m/s) and no clear stress-dependent trend is evident. However, this comparison is limited, as most individual sampling locations are represented by only one or two stress levels. Published results from the Lausen borehole (Crisci et al., 2019), combining oedometer- and constant-head-derived K across both bedding orientations, follow a power-law relationship with vertical effective stress, given by $K=(1.32\times10^{-12})\times \sigma'_v{}^{-1.085}$, fitted over a broader range of approximately 0.1 to 50 MPa (see Crisci et al., 2019; Figure 10). Evaluated at effective stresses ≥5 MPa, comparable to the OPA data discussed above, this relationship predicts a change of only ~1 order of magnitude (approximately 10^{-13} to 10^{-14} m/s). The larger apparent stress sensitivity implied when including the lowest effective stresses (<5 MPa) is attributed by Crisci et al. (2019) to micro-fissuring associated with exhumation decompaction, rather than to stress-driven matrix compaction alone.

AMA data show a systematic decline in K with increasing effective confining stress that persists at least up to ~10 MPa across all tests. Beyond 10 MPa, the trend becomes inconsistent between the different samples, with

Formatiert: Tiefgestellt
Formatiert: Tiefgestellt
Formatiert: Hochgestellt
Formatiert: Hochgestellt
Formatiert: Hochgestellt
Formatiert: Hochgestellt
Formatiert: Hochgestellt
Formatiert: Hochgestellt

some continuing to decline while others flatten. As observed for Lausen, the lowest effective stress level (1 MPa) yields markedly elevated K values across all AMA samples, plausibly reflecting a comparable exhumation/low-stress microfissuring effect. Excluding this lowest stress level, AMA hydraulic conductivities across the tested range (5 to 20 MPa) span approximately 1.5 orders of magnitude.

Under quasi-constant effective confining stress conditions, To-Do and BCF samples span a hydraulic conductivity range up to one order of magnitude between 3.3×10^{-14} to 1.2×10^{-13} m/s and 1.1×10^{-14} to 1.3×10^{-13} m/s, respectively.

~~Figure 8 shows hydraulic conductivity plotted against the respective effective confining stress. For OPA, samples from different locations cover a stress range of 5 – 15 MPa, with all data points clustering within two orders of magnitude (10^{-14} to 10^{-12} m/s). Within this range, no clear stress-dependent trend is evident. However, the comparison is limited because only a few data points originate from the same sampling location and depth. Additional results from the Lausen borehole confirm a similar hydraulic conductivity range, despite spanning a broader stress interval of 0 – 50 MPa (Crisci et al., 2019). In that case, the hydraulic conductivity decreased systematically with increasing effective stress, reflecting compaction-related reduction in void ratio. The AMA data also show an initial decline in K with increasing stress, but this trend vanishes at confining stresses above ~5 MPa (10 – 20 MPa range). Overall, AMA hydraulic conductivities fall within the same two-order magnitude window (10^{-12} to 10^{-14} m/s) as the OPA data. Taken together, the compiled data suggest that, across all studied formations, hydraulic conductivity consistently falls within a range of two orders of magnitude, despite applied effective stresses varying between 1 and 50 MPa.~~

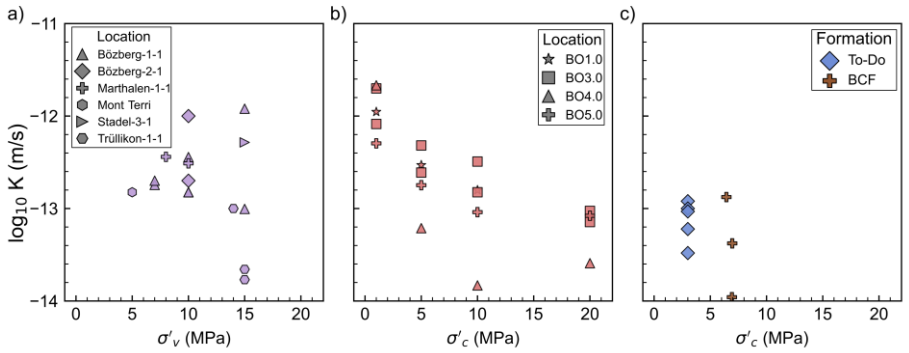
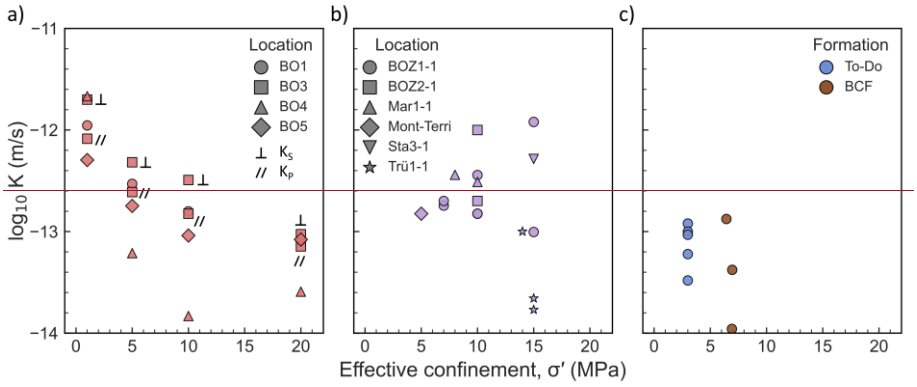


Figure 8 Log hydraulic conductivity versus the applied effective stress during hydraulic laboratory experiments: a) constant-head tests executed on OPA samples from several (borehole) locations at variable vertical effective stress (σ'_v) stages during oedometer tests; b) constant-head test results of AMA samples from different drilling locations at varying effective confining stress stages; c) results from pressure-pulse decay experiments conducted on To-Do and BCF specimen at quasi static effective confining stress.

Formatiert: Nicht vom nächsten Absatz trennen

Formatiert: Beschriftung, Abstand Vor: 0 Pt., Nach: 0 Pt.

Formatiert: Tiefgestellt



~~*Figure 8 Log hydraulic conductivity versus the applied effective confinement stress during permeameter experiments. Formations are color-coded, while distinct marker symbols are used to differentiate individual sample locations for OPA and AMA. OPA locations: BOZ=Bözberg, Mar=Marthalen, Sta=Stadel, Trü=Trüllikon. For AMA data the sample orientation with respect to bedding is indicated, where samples of both orientations (vertical and horizontal to bedding) were tested.*~~

4.3.4 Summary and baseline definition

The compiled dataset was evaluated with respect to potential factors influencing hydraulic conductivity in order to establish a baseline definition of its naturally occurring variability. This is particularly important because the data covers six formations, each with intrinsic internal heterogeneity (e.g., due to lateral facies changes or vertical lithological variation), which introduces natural bias. The analysis, therefore focused on parameters that could be quantitatively assessed from the available data, namely: (a) the measurement scale (centimetres in the laboratory versus few metres to several decametres in field investigations), (b) bedding-related hydraulic anisotropy, and (c) the applied effective stress conditions during laboratory ~~permeameter tests~~experiments, all of which are known to exert variable influence on measured hydraulic conductivity.

The natural hydraulic anisotropy with respect to bedding results from the preferential orientation of clay platelets parallel to stratification, typically yielding ratios of horizontal (K_P) to vertical (K_S) conductivity between 1.5 and 5 (Clennell et al., 1999; Bastiaens et al., 2007; Neuzil, 2019). Formation-specific anisotropy ratios (K_P/K_S) in the compiled dataset range from 1.07 (OPA) and 1.23 (COx) to 1.55 (AMA) and 2.72 (Boom Clay) (Sect. 4.3.2), i.e., generally at or below the lower end of previously reported values, with OPA and COx showing near-isotropic behaviour. Relative to the two-order-of-magnitude natural variability envelope defined below, a factor of up to ~2.7 between K_P and K_S is comparatively minor. ~~The compiled data shows a median K_P/K_S ratio of approximately 3, in good agreement with this range, indicating that anisotropy introduces only a minor influence on the overall comparability of hydraulic conductivity values.~~ Hydraulic conductivity from *in situ* tests, such as packer experiments, mostly conducted in vertical boreholes, predominantly reflect ~~K_P (or~~ a mixed response of both bedding orientations, and can therefore be expected to fall between laboratory-derived K_P and K_S values~~where bedding orientations fall between the two end members), and can therefore be expected to yield slightly higher conductivities than laboratory-derived K_S values~~.

Formatiert: Tiefgestellt
Formatiert: Tiefgestellt
Formatiert: Tiefgestellt
Formatiert: Tiefgestellt
Formatiert: Tiefgestellt
Formatiert: Tiefgestellt

The influence of measurement scale, however, proved to be more complex. Within the shallow, stress-relieved interval affected by decompaction (up to 100 m below surface), a strong dependence of hydraulic conductivity on the scale of investigation was evident, both between laboratory and field measurements and among field intervals of varying length. Below this zone, scale effects essentially vanish: across all formations, laboratory and *in situ* conductivities converge and fall predominantly within a range between 10^{-14} and 10^{-12} m/s. A similar range emerges when considering the influence of effective ~~confining~~ stress conditions during ~~permeameter~~ laboratory testing. Despite effective stress variations (e.g., vertical effective stress ranging from 1 to 50 MPa)~~,~~ matrix conductivities consistently remain within this same range.

~~Therefore~~Following these observations, we define a natural variability envelope for the undisturbed matrix hydraulic conductivity of argillaceous formations between 10^{-14} and 10^{-12} m/s. This range represents the baseline against which deviations caused by near-surface decompaction, fracture development, or deep-burial alteration will be evaluated in the discussion.

4.4 Mineralogical formation characteristics

Bulk mineralogical data provide quantitative information on clay minerals, carbonates, and framework silicates (quartz + feldspar + accessories). Overall, the dataset captures a wide range of mineralogical compositions (Fig. 9), with Boom Clay and To-Do representing the extremes of carbonate-poor and carbonate-rich endmembers, respectively. Clay mineral content is highest in OPA and AMA, lowest in To-Do, while quartz + feldspar + accessory contents are generally inversely related to carbonate abundance. Generally, the mineralogical ranges of the present dataset align with those reported in the Clay Club Catalogue (OECD and NEA, 2022).

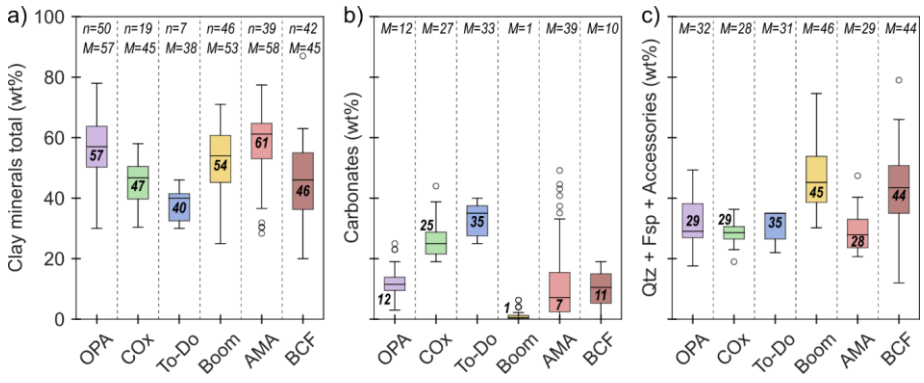


Figure 9 Bulk mineralogical composition of the studied argillaceous formations based on the compiled dataset. Boxplots show the distribution of a) total clay minerals, b) carbonates, and c) quartz + feldspar + accessory minerals (all in wt%). Boxes represent the interquartile range (IQR) with the median as a horizontal line and bold number in or next to the boxes, whiskers indicate 1.5× IQR, and circles denote outliers. The data population (n) and mean (M) are given ~~on to of~~for the individual boxplots.

4.5 Petrophysical formation characteristics

The petrophysical properties of the investigated formations show pronounced inter-formational variability (Table ~~7~~6 and Fig. 10). Mean porosity values in indurated and over-consolidated formations range from below 2 % in the

BCF over ~8 % in To-Do, 11 % in AMA, 12 % in OPA, and 15 % in COx. The Boom Clay displays distinctly higher porosities of up to 40 %, reflecting its relatively shallow burial depth and limited diagenetic overprint. Grain densities show little variability across formations, with means clustering around 2.66 – 2.72 g/cm³, consistent with typical argillaceous mineral assemblages (Totten et al., 2002). Bulk densities generally follow porosity trends. High-porosity formations such as the Boom Clay exhibit markedly lower bulk densities (~1.66 g/cm³), whereas the more compacted and diagenetically altered units (BCF, COx, To-Do, OPA, AMA) show bulk densities in the range of 2.42 – 2.46 g/cm³. Again, the BCF represents a lower-end member with a bulk density around 2.65 g/cm³.

Table 7~~6~~ Selected petrophysical characteristics of the investigated formations. The values represent the mean of the sampled data range as well as their standard deviation: porosity (Φ), grain density (ρ_{grain}), and dry bulk density (ρ_{bulk}). The data population (n) is additionally given for each parameter and formation.

Formation	Φ (%)	n	ρ_{grain} (g/cm³)	n	ρ_{bulk} (g/cm³)	n
OPA	11.58 ± 1.47	36	2.72 ± 0.03	48	2.45 ± 0.03	28
COx	14.72 ± 2.98	51	2.66 ± 0.06	29	2.23 ± 0.03	7
To-Do	7.71 ± 1.99	138	2.70 ± 0.01	12	2.46 ± 0.04	22
Boom	36.36 ± 10.31	15	2.71 ± 0.03	7	1.66 ± 0.04	12
AMA	10.83 ± 2.56	46	2.72 ± 0.04	42	2.42 ± 0.08	43
BCF	1.90 ± 0.69	6	2.77 ± 0.01	3	2.65 ± 0.05	3

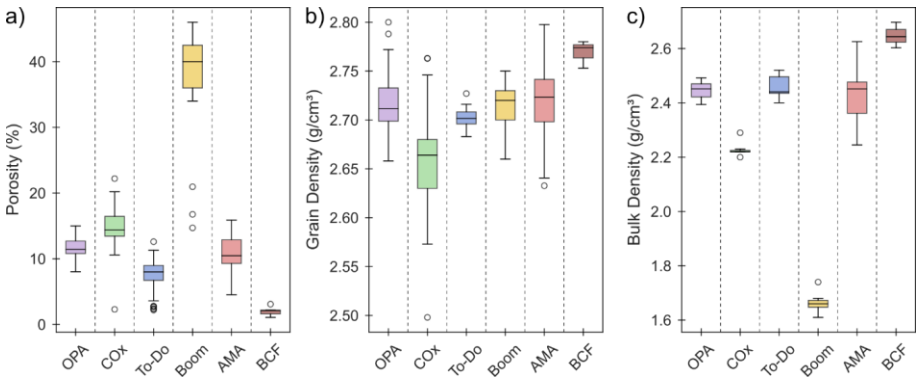


Figure 10 Selected petrophysical characteristics of the compiled data for all investigated formations: a) porosity, b) grain density, c) bulk density.

Across the investigated formations, mean porosity values show a broadly positive correlation with laboratory-measured hydraulic conductivity (Fig. 11a), reflecting pore space closure in response to mechanical compaction and cementation (Mazurek et al., 2011). ~~as expected while~~Conversely, hydraulic conductivity exhibits a negative correlation with bulk density (Fig. 11b). However, COx shows slightly lower mean K compared to OPA and AMA despite a generally higher porosity of about 3 – 4 %, illustrating that K may additionally be influenced by factors such as pore size distribution, mineralogical composition and spatial mineral distribution (Gaus et al., 2022 and references therein).~~if porosity alone would determine hydraulic conductivity, COx would be expected to show higher K values than the OPA and AMA, both of which have porosity values approximately 3 – 4 % lower than COx. Instead, COx generally exhibits lower hydraulic conductivity.~~ Similarly, data from the BCF show slightly higher hydraulic conductivity than the Toarcian-Domerian formation, despite the BCF's distinctly lower porosity and higher bulk density.

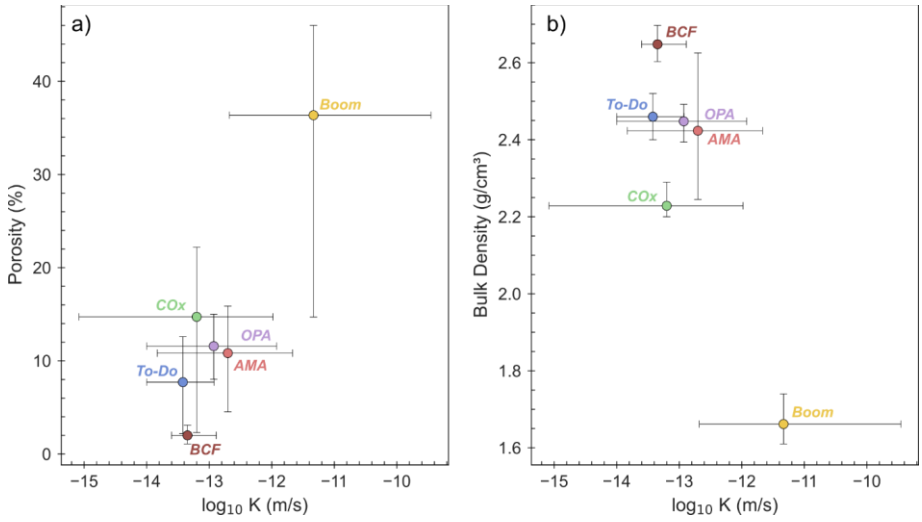


Figure 11 Comparison of petrophysical properties versus the mean $log_{10}K$ measured in laboratory conditions across the investigated formations: a) porosity versus hydraulic conductivity; b) bulk density versus hydraulic conductivity. Markers represent mean values while whiskers indicate the minimum and maximum range observed. Depth filtering was applied to the OPA dataset to exclude data shallower than 50 m in order to avoid effects of weathering.

4.6 Hydraulic conductivity and porosity with respect to maximum burial

The formations considered in this study experienced markedly different burial and uplift histories, with maximum burial depths ranging from only several decametres below ground (Boom Clay) to several kilometres (Fig. 12). Four formations (OPA, To-Do, AMA, BCF) reached depths exceeding 1,000 m during their geological evolution, followed by partial to significant uplift, resulting in pronounced over-consolidation. Among these, the AMA shows the largest internal burial depth variability, with reconstructed maximum burial depths between 1,400 m and 3,300 m (Castro-Vera et al., 2024; Burchartz et al., 2026), while the OPA reached depths of 1,350 – 1,700 m (Mazurek et al., 2006). The BCF represents the deepest end-member, with burial depths of up to 4,500 m.

The porosity distribution follows a clear burial-related trend with a good~~strong~~ exponential fit (R^2=0.80~~3~~; Fig. 12b), representing systematic pore-space reduction as a response to compaction and cementation processes along gradual burial (Addis and Jones, 1985; Jones and Addis, 1985). A slight deviation from this trend is observed within the AMA dataset, where porosity increases slightly between burial depths of 2,440 m (BO4.0) and 3,300 m (BO5.0). Castro-Vera et al. (2024) attributed this to local overpressure development at the BO5 site, which likely reduced effective stress during burial. Porosities in AMA and OPA agree closely for sites that experienced similar burial depths (e.g., BO1 ≈ Jura Ost; BO2 ≈ Mont Terri).

Hydraulic conductivity exhibits a less pronounced, more complex relationship with maximum burial depth (Fig. 12a). A substantial decrease in laboratory-derived hydraulic conductivity is evident between the shallowly buried Boom Clay and the more deeply buried Callovo-Oxfordian argillite, which faced a maximum burial depth of approximately 850 m. This pronounced decline vanishes from burial depths beyond ~1,000 m. Instead, subtle intra-formational trends can be identified. In the OPA, hydraulic conductivity decreases progressively from the

Mont Terri URL to the deeper Jura Ost, Zürich Nordost, and Nördlich Lägern sites. A similar, though gentler, decrease is observed in the AMA data, with a slight rise in hydraulic conductivity at the site which experienced the deepest maximum burial (BO5.0, 3,300 m), mirroring the porosity pattern and suggesting the same influence of local overpressure (Gaus et al., 2022; Castro-Vera et al., 2024; Burchartz et al., 2026).

For formations that experienced maximum burial depths <2,000 m, laboratory-derived and *in situ* hydraulic conductivity show a close agreement, indicating consistent matrix and bulk hydraulic properties at depth. Here, discrepancies are smaller than one order of magnitude and therefore lie well within the prior defined natural variability of K. In contrast, a divergence between laboratory- and field-scale hydraulic conductivity values emerges in formations with burial depths ≥2,000 m, notably in the To-Do and BCF. The latter shows differences of several orders of magnitude between laboratory and field measurements. *In situ* AMA data were excluded here, as near-surface processes, particularly decompaction, produced elevated hydraulic conductivity.

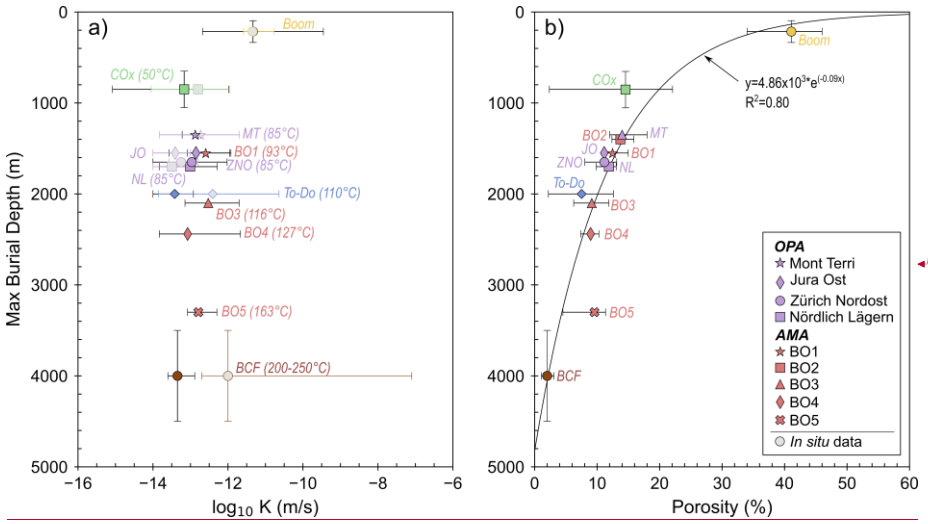
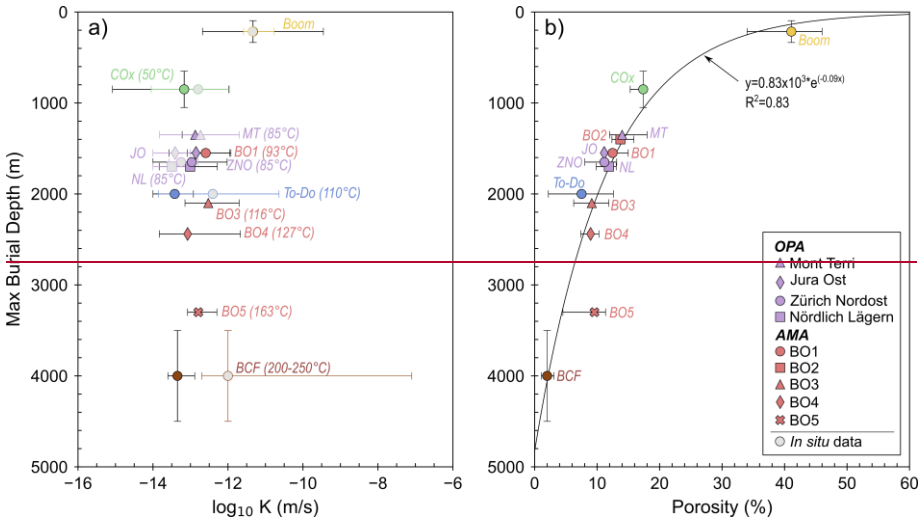


Figure 12 Relationships of log hydraulic conductivity and total porosity with maximum burial depth estimations: a) log hydraulic conductivity versus maximum burial depth for laboratory (coloured markers) and in situ measurements (grey filled markers). Given temperatures represent estimates on maximum temperatures reached during burial. Data of the OPA is given in four groups: MT represents data from the Mont Terri URL, JO, ZNO, and NL is data derived from boreholes drilled in the siting regions Jura Ost, Zürich Nordost, and Nördlich Lägern, respectively; b) total porosity versus estimated maximum burial depth. Data from present day depth <100 m was excluded to avoid decompaction and weathering effects. Horizontal error bars represent the full range of compiled data (min, max), and vertical error bars indicate uncertainty in maximum burial depth estimates. Marker positions for Boom, COx, OPA, AMA, To-DO, and laboratory derived BCF represent the geometric mean value of K. The presented in situ BCF as well as its max. burial depth range is after OECD and NEA (2022); here the marker position was chosen based on the given K best estimate and the mean of the reported max. burial depth range (3,500 – 4,500 m). Please note that Boom data originates from different boreholes but was plotted as a single point with the entire data-range for better overview.

Formatiert: Nicht vom nächsten Absatz trennen

Formatiert: Beschriftung, Abstand Vor: 0 Pt., Nach: 0 Pt.



740 *Figure 12 Relationships of log hydraulic conductivity and total porosity with maximum burial depth estimations: a) log hydraulic conductivity versus maximum burial depth for laboratory (coloured markers) and in situ measurements (grey filled markers). Given temperatures represent estimates on maximum temperatures reached during burial. Data of the OPA is given in four groups: MT represents data from the Mont Terri URL, JO, ZNO, and NL is data derived from boreholes drilled in the siting regions Jura Ost, Zürich Nordost, and Nördlich Lägern, respectively; b) total porosity versus estimated maximum burial*
745 *depth. Data from present day depth <100 m was excluded to avoid decompaction and weathering effect. Horizontal error bars represent the full range of compiled data (min, max), and vertical error bars indicate uncertainty in maximum burial depth estimates. Marker positions for Boom, Cox, OPA, AMA, To-DO, and laboratory derived BCF represent the geometric mean value of K.. The presented in situ BCF as well as its max. burial depth range is after OECD and NEA (2022); here the marker position was chosen based on the given K best estimate and the mean of th reported max. burial depth range (3,500*
750 *4,500 m).Table 8 Summary of statistical values (geometrical mean hydraulic conductivities and sample sizes indicated by hashtag in brackets behind the respective K-value) considered in Fig. 12a. For OPA and AMA the individual sampling/testing locations are given. For OPA they are classified with respect to the respective siting-region.*

Formation	Siting area/Location	Borehole	Geom. Mean K_{lab} (m/s)	Geom. Mean $K_{in\ situ}$ (m/s)
Boom			4.65×10^{-12} (#269)	4.53×10^{-12} (#30)
COx			6.31×10^{-14} (#47)	1.59×10^{-13} (#30)
OPA	Mont Terri		1.34×10^{-13} (#4)	1.86×10^{-13} (#15)
	Jura Ost (JO)		1.40×10^{-13} (#25)	3.90×10^{-14} (#9)
		Rinken	-	8.94×10^{-14} (#2)
		Bözberg-1-1	1.36×10^{-13} (#15)	5.24×10^{-14} (#3)
		Bözberg-2-1	1.46×10^{-13} (#10)	2.10×10^{-14} (#4)
	Nördlich Lägern (NL)		9.80×10^{-14} (#11)	3.46×10^{-14} (#9)
		Bachs-1-1	2.38×10^{-13} (#2)	4.47×10^{-14} (#2)
		Bülach-1-1	1.03×10^{-13} (#2)	-
		Stadel-2-1	1.57×10^{-13} (#2)	2.90×10^{-14} (#3)
		Stadel-3-1	5.57×10^{-14} (#5)	3.46×10^{-14} (#4)
	Zürich Nordost (ZNO)		1.08×10^{-13} (#25)	5.60×10^{-14} (#11)
		Trüllikon-1-1	6.68×10^{-14} (#13)	3.46×10^{-14} (#2)
		Marthalen-1-1	1.83×10^{-14} (#12)	4.93×10^{-14} (#3)
		Rheinau-1-1	-	4.58×10^{-14} (#2)
		Benken	-	7.83×10^{-14} (#4)
AMA		BO1	2.55×10^{-13} (#4)	-
		BO3	2.98×10^{-13} (#8)	-
		BO4	8.40×10^{-14} (#4)	-
		BO5	1.62×10^{-13} (#4)	-
To-DO			3.80×10^{-14} (#8)	3.92×10^{-13} (#6)

Formatiert: Beschriftung, Nicht vom nächsten Absatz trennen

Formatiert: Tiefgestellt

Formatiert: Tiefgestellt

Formatiert: Zeilenabstand: einfach

Formatierte Tabelle

Formatiert: Zeilenabstand: einfach

Formatiert: Hochgestellt

Formatiert: Hochgestellt

Formatiert: Zeilenabstand: einfach

Formatiert: Hochgestellt

Formatiert: Hochgestellt

Formatiert: Zeilenabstand: einfach

Formatiert: Links, Zeilenabstand: einfach

Formatiert: Zeilenabstand: einfach

Formatiert: Links, Zeilenabstand: einfach

Formatiert: Zeilenabstand: einfach

Formatiert: Zeilenabstand: einfach

BCF	4.50×10^{-14} (#3)	-

Formatiert: Zeilenabstand: einfach

Formatiert: Englisch (Vereinigtes Königreich)

Formatiert: Standard

5 Discussion

Collectively, the investigated formations represent a continuum of diagenetic maturity, from the unlithified, stiff, slightly over-consolidated Boom Clay Formation to slightly or moderately indurated claystones (e.g., COx and OPA, respectively), to very highly indurated claystones such as the Boda Claystone Formation, which experienced burial to ~4.5 km before exhumation.

The compiled porosity data clearly follows the expected burial trend, with progressive pore space reduction accompanying mechanical compaction and cementation. The hydraulic conductivity initially shows a ~~broadly~~ comparable ~~similar pattern, with a marked~~ decrease between the Boom Clay and COx that faced maximum burial of around 850 m depth. However, beyond this depth, the trend flattens. For the mechanically compacted and lithified formations~~,~~ (CO~~o~~x, OPA, AMA, To-Do, and BCF) ~~(e.g., Cox, OPA),~~ the vast majority of matrix hydraulic conductivity determined from laboratory tests fall within a range of 10^{-14} to 10^{-12} m/s, independent of site, formation, or test conditions. This range, previously defined as the natural variability envelope, likewise characterizes the hydraulic behaviour at the rock mass scale for formations that faced maximum burial <2,000 m, namely Cox and OPA, in the absence of near-surface perturbations such as weathering or decompaction.

At greater burial depths (≥ 2,000 m; To-Do, BCF), a second systematic divergence emerges between matrix and field-scale hydraulic conductivity. While laboratory-derived matrix hydraulic conductivity remains within the natural variability range, *in situ* data indicate elevated values ~~partly~~ up to several orders of magnitude ~~higher~~. This shift was already highlighted by Mazurek et al.~~,~~ (2009), who described a two-stage evolution of hydraulic conductivity in argillaceous formations: (i) a continuous decrease with burial, porosity loss, and cementation up to depths of ~2,000 m, and (ii) a subsequent increase at greater burial depths, reflecting the growing hydraulic role of open fractures as matrix permeability becomes negligible and self-sealing capacity diminishes due to a lower amount or absence of swellable clay minerals. Their synthesis further highlighted that the discrepancy between laboratory and *in situ* measurements is small or absent in less indurated formations (e.g., Boom Clay, OPA), whereas in deeply buried, strongly over-consolidated formations (e.g., BCF), fracture flow increasingly governs bulk hydraulic behaviour.

The observations from this study align closely with those outlined by Mazurek et al. (2009). Below the shallow decompaction zone, matrix and field-scale hydraulic conductivity converges, indicating diffusion-dominated conditions and efficient self-sealing. In contrast, at high degrees of induration (To-Do and BCF), fractures can become the dominant fluid pathways, and the ability of the matrix to re-establish sealing after stress release or deformation is strongly reduced.

Potential causes and the principal processes controlling these past and present depth-dependent trends, including the mechanisms of self-sealing, the development of the decompaction zone, and the transition from matrix- to fracture-dominated flow, are discussed in the following sections with respect to the individual formation characteristics.

Several aspects of the compiled dataset bear uncertainty and necessitate caution when interpreting these trends. In particular, the divergence between matrix and field-scale hydraulic conductivity for formations with maximum burial depths ≥2,000 m is based on a comparatively limited number of formations and measurements (To-Do, BCF), and the natural variability envelope itself is derived from unevenly distributed formation and testing conditions. These and further limitations, including uncertainties in burial depth reconstruction and incomplete formation-specific data on pore structure and swelling clay mineral content, are discussed in sub-section 5.4 and should be kept in mind throughout the following sections.

5.1 Self-sealing characteristics of investigated formations

The development of discontinuities such as fractures, joints, and bedding planes enhances secondary permeability and can significantly increase fluid flow through the rock mass (Neuzil, 1994; Ishii et al., 2011; Neuzil, 2015, 2019). Argillaceous formations, however, possess a remarkable capacity to self-seal such dilatant features over time, a key property that underpins their consideration as potential host rock for radioactive waste disposal (Bock et al., 2010). This self-sealing capacity arises from several mechanisms, including stress-state-dependent mechanical fracture closure (increased effective normal stress), swelling of clay minerals, mineral precipitation, creep deformation, and shearing or slaking processes (Bock et al., 2010; Di Donna et al., 2022; Berry et al., 2025). Bock et al.~~,~~ (2010) synthesized numerous studies on the self-sealing behaviour of most of the formations investigated here (excluding the AMA), showing that self-sealing occurs across all formations, but varies on both spatial and temporal scales. Differences in sealing effectiveness are strongly controlled by clay mineralogy, degree of induration, and porewater chemistry (Bock et al., 2010). A detailed and very recent overview of self-sealing processes in argillaceous media is provided by Berry et al.~~,~~ (2025).

In the soft Boom Clay, self-sealing is primarily governed by clay mineral swelling (discrete s~~S~~mectite fraction of the clay mineral components is at 7 – 24 wt.% and 7 – 23 wt.% i~~I~~llite-s~~S~~mectite interlayers; after: Zeelmaeker et al. 2015) and occurs over short time periods, leading to a near-complete recovery of the initial matrix hydraulic properties. Within the SELFRAC project, this process was shown to be efficient across multiple scales, although complete mechanical healing remains limited (Bastiaens et al., 2007; Van Geet et al., 2008; Gonzalez-Blanco et al., 2024). The close agreement between laboratory and *in situ* hydraulic conductivity measurements further underlines the strong self-sealing capacity of Boom Clay, indicating effective closure of potential fractures at the rock-mass scale. For the moderately indurated COx and OPA formations, numerous studies have examined self-sealing behaviour with a focus on swelling and mechanical consolidation processes (Van Geet et al., 2008; Zhang, 2010, 2011; Di Donna et al., 2022; H. Wang et al., 2024; C. Wang et al., 2025). Swelling-induced sealing is efficient in both formations, and depending on mineralogical composition and confinement, hydraulic conductivity can be restored to values close to the initial matrix level (Voltolini & Ajo-Franklin, 2020; Wang et al., 2022; 2025; Zhang & Talandier, 2023). Discrete swellable clay mineral phases (mostly s~~S~~mectite) occur in COx at ~11 to 26 wt.% of the clay mineral fraction and as i~~I~~llite-s~~S~~mectite (I-S) mixed layers of >20 wt.%(Hu et al. 2014; Wang et al. 2022). While OPA is depleted in discrete smectite phases, it contains 10 to 38 wt% I-S (Kneuker et al., 2023, 2026).

In the moderately indurated formations (~~Clay,~~ COx, OPA), self-sealing typically occurs over time spans of months to a few years (Bock et al., 2010) and is dominated by swelling, consolidation, and creep mechanisms (Bastiaens

Feldfunktion geändert

et al., 2007). This is reflected in the presented dataset, which shows close agreement between laboratory and field-scale hydraulic conductivity values, indicating efficient sealing of natural or excavation-induced discontinuities~~.~~ provided the absence of near surface perturbations e.g.,~~i.e.~~ due to decompaction and weathering~~below approximately 250 m depth~~. This interpretation is further corroborated by the findings of Gautschi~~,~~ (2001), who, based on observations from more than 6.6 km of tunnel sections excavated through the Opalinus Clay in northern Switzerland, reported that even in faulted and folded domains only negligible water inflows occurred. Notably, all recorded inflows were restricted to sections with an overburden of less than approximately 200 m. In contrast, self-sealing appears to be diminished in the shallow OPA zone, as evidenced by elevated and variable hydraulic conductivity values in shallow boreholes in the Swabian Alb (Hekel, 1994) and the Lausen borehole (Vogt et al., 2017; Crisci et al., 2019). This depth contrast highlights the role of confinement, which in combination with clay mineral swelling, results in effective self-sealing processes (Voltolini and Ajo-Franklin, 2020).

Toarcian-Domerian argillites exhibit ~~generally~~ overlapping *in situ* and laboratory hydraulic conductivity ranges, mostly within the the pre-defined natural variability ~~range~~. However, localized zones of higher conductivity (10^{-11} m/s) identified in field experiments suggest the presence of unsealed, hydraulically active fractures (Boisson et al., 2001). Additional evidence of water inflow zones in boreholes (Beaucaire et al., 2008) and minor moist areas in the Tournemire URL (Mazurek et al., 2009) supports this interpretation. These observations indicate a lower self-sealing efficiency compared to the less indurated formations (Boom Clay, COx, and OPA). According to Bock et al. (2010), a conservative threshold of approximately 40 wt.% clay mineral content marks a threshold below which self-sealing becomes ineffective. The mineralogical composition of To-Do lies near this threshold, suggesting that swelling-driven sealing is less pronounced. In addition, swelleable clay mineral phases lay at ~9 – 15 wt.% of the total clay mineral fraction, notably below those of Boo~~OO~~m~~M~~, COx, and OPA (Bock et al., 2010). Geng et al.~~,~~ (2021) observed substantial sealing during compaction-creep deformation in To-Do samples, but primarily under coupled THCM conditions corresponding to simulated depths around 3.8 km, i.e., conditions not relevant for repository environments.

In the case of the BCF, the highly indurated nature and general depletion of swellable clay minerals (s~~S~~mectite content near the detectable limit of >1 wt.%) do not favour rapid self-sealing (Kovács, 2001). The pronounced discrepancy between small-scale (laboratory) and large-scale (rock mass) hydraulic conductivity is evident in the compiled dataset and likely reflects ~~insufficient~~ low self-sealing capacity. However, Kovács (2001) reported partial sealing due to degradation of non-swelling clay minerals and mineral precipitation within joints. Such processes may contribute to very long-term sealing and should be considered in detailed repository performance assessments~~.~~ ~~However,~~ although their timescales likely exceed the time-span over which a host-rock is required to prevent radionuclide migration to the environment (e.g., 1 Ma in Germany; ~~(~~StandAG, 2017) ~~operational period of a repository~~ (Bock et al., 2010). The transition from sedimentary to metamorphic rock marks the ultimate threshold beyond which self-sealing becomes ineffective~~, as swelling clay minerals are largely absent~~ (Bock et al., 2010).

The self-sealing behaviour of the Amaltheenton Fm has not yet been characterized but is currently being investigated within the framework of the MATURITY project (Burchartz et al., 2026). ~~Quelle ÄNDERN!~~

5.2 The role of maximum burial depth

The general diagenetic changes occurring during progressive burial were outlined in the introductory chapter. The compiled data clearly demonstrate that maximum burial exerts a lasting influence on both the hydraulic and petrophysical characteristics of the investigated formations. This influence is particularly evident in the ~~strong~~ relationship between porosity (or inversely, bulk density) and maximum burial depth observed across the dataset. An initial porosity loss exceeding 20 % is observed between the Boom Clay and the COx, corresponding to a differential burial of approximately 600 m. This highlights the pronounced porosity reduction caused by mechanical compaction during early burial diagenesis (Athy, 1930; Addis and Jones, 1985; Cripps and Czerewko, 2017; Ewy et al., 2020). At this stage, the most substantial reduction in hydraulic conductivity is also observed, while both the porosity-depth and hydraulic conductivity-depth trends flatten with further burial. The initial pore closure associated with mechanical compaction thus represents an ~~first-order~~important control on the low hydraulic conductivity characteristic of argillaceous formations. Neuzil, (1994) indicates~~demonstrated~~ the existence of a log-linear relationship between porosity and permeability/hydraulic conductivity across a broad range of argillaceous formations, a trend also reflected in the data compiled for this study. This relationship is directly resolved within OPA, where region-specific porosity and laboratory K show a strong log-linear correlation (R^2 = 0.81, n = 4; Fig. 13). A comparable, though less consistent, relationship is observed for AMA. Across the investigated formations, a broad porosity-K relation can be observed that is comparatively weaker (Fig. 11a), reflecting the additional influence of pore size distribution, mineralogical composition, and grain size distribution across formations of differing genesis. This is specifically evident from the COx data that shows a slightly lower geom. mean K (6.31×10^{-14} m/s) while exhibiting higher mean porosity (14.72 %) compared to OPA (1.18×10^{-13} m/s; 11.58 %). This might be as a result of early diagenetic precipitated non-biogenic carbonates that potentially results in the clogging of pore throats, reducing water accessible flow paths and associated K (Esteban et al., 2007; Yven et al., 2007; Menaceur et al., 2015; Robinet et al., 2015). ~~Accordingly, hydraulic conductivity would be expected to decrease further with continued pore-space reduction beyond approximately 850 m burial. This~~ Nevertheless, the general reduction in K with decreasing porosity across the investigated formations can be traced~~is generally consistent across the investigated formations and observational scales (laboratory versus *in situ*) up~~ to maximum burial depths of around 2,000 m, although the trend becomes less pronounced with depth. Beyond this threshold, no further systematic decrease in hydraulic conductivity is apparent. It can therefore be concluded that hydraulic conductivity remains positively correlated with porosity down to porosity values of roughly 10 %, or better burial depth <2,000 m, which is in in agreement with previous findings by Mazurek et al. (2011).

Formatiert: Hochgestellt

Formatiert: Hochgestellt

Formatiert: Hochgestellt

Formatiert: Schriftart: Kursiv

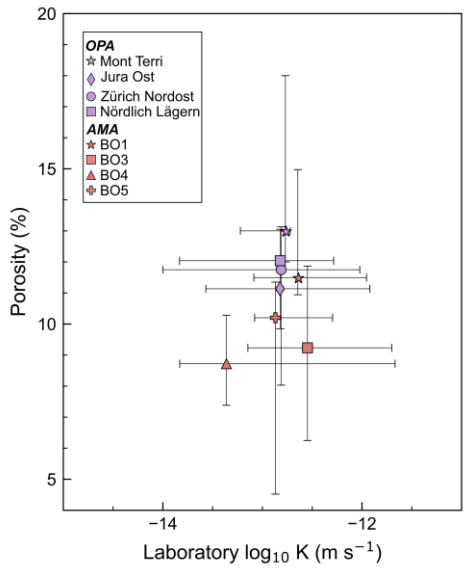


Figure 13 Porosity versus laboratory derived hydraulic conductivity plot for OPA and AMA at different locations. Markers represent the geometric mean while whiskers show the range between minimum and maximum values.

Formatiert: Beschriftung

Formatiert: Abstand Vor: 0 Pt., Rahmen: Oben: (Kein Rahmen), Unten: (Kein Rahmen), Links: (Kein Rahmen), Rechts: (Kein Rahmen)

At maximum burial depths exceeding 2,000 m, a divergence emerges between laboratory-derived matrix hydraulic conductivity and field-derived rock mass values, with the latter increasing up to several orders of magnitude. This divergence likely reflects the growing hydraulic influence of fractures superimposed on an otherwise low-conductivity matrix (Laubach et al., 2009; Gale et al., 2014). As discussed in ~~Chapter~~ section 5.1, burial depth also exerts a strong control on the self-sealing efficiency of argillaceous formations, which progressively lose their swelling capacity with increasing induration. This loss is closely linked to the time- and temperature-dependent transformation of smectite to the thermally more stable illite via an intermediate mixed-layer (I/S) phase (Pollastro, 1993; Peltonen et al., 2009), described by the reaction:

$$smectite + K^{+} \xrightarrow{time\&temperature} illite + quartz + nH_2O \quad (32)$$

This reaction results in the release of interlayer water, the crystallization of authigenic quartz, the formation of smaller and stiffer crystal structures (Carcione et al., 2022), and consequently, further porosity loss, increased brittleness, reduced ductility (Berthonneau et al., 2017), and diminished swelling potential. In contrast to moderately indurated formations such as the COx and OPA, where effective self-sealing can counteract long-term fracture permeability, highly indurated formations such as the BCF exhibit the combined effects of increased brittleness and strongly reduced swelling potential, preventing efficient fracture sealing. As noted by Mazurek et al.~~,~~ (2009), the To-Do formation represents a transitional case, where the indurated matrix allows for fracturing while retaining a limited, though not entirely lost, self-sealing capacity.

5.3 The role of present-day depth

A pronounced present-day depth trend of hydraulic conductivity reduction is apparent from the indurated and over-consolidated formations, which is in agreement with global datasets published earlier (see e.g., Appel and Habler, 2001; Batlle-Aguilar et al., 2016; Asem and Gardoni, 2022). No pronounced depth trend could be observed on the soft Boom Clay. In the (moderately) indurated and over-consolidated formations OPA and AMA, elevated and variable *in situ* hydraulic conductivity is observed in the upper metres to decametres of depths. This trend diminishes with depth. At depths >250 m *in situ* and laboratory derived hydraulic conductivity overlaps in all formations that faced experienced maximum burial <2,000 m. Stronger indurated formations (To-Do and BCF) showed scale dependency of the hydraulic conductivity with small scale (laboratory) values fitting the natural variability (10^{-14} to 10^{-12} m/s), while large scale (*in situ*) hydraulic conductivity can be substantially higher. Based on these observations two distinct domains depending on the extent of decompaction can be differentiated.:

5.3.1 Decompaction and weathering zone

The first 30 – 100 m are characterized by *in situ* hydraulic conductivity values derived from packer tests that span up to ten orders of magnitude. In the shallow Opalinus Clay (OPA) of northern Switzerland, penetrated by the Lausen borehole, hydraulic conductivity decreases sharply within the upper 30 m, and beyond this depth the values become similar to those obtained from laboratory measurements (Vogt et al., 2017; Crisci et al., 2019). In contrast, in the Swabian Alb (Germany), elevated hydraulic conductivity values are observed at depths of around 40 – 60 m (Hekel, 1994; Vogt et al., 2017). In both cases, the enhanced hydraulic conductivity is linked to the degree of fracturing, which decreases with depth (Hekel, 1994; Vogt et al., 2017; Mazurek et al., 2023). For the Lausen borehole, the high degree of fracturing in the upper 30 m has been attributed to extensional fractures formed as a result of reduced vertical effective stress during uplift (Vogt et al., 2017). Aside from hydraulically active fractures, diffusive transport still remains the dominant transport mechanism governing solute exchange between fractures and matrix, even in the weathered Opalinus Clay encountered in the Lausen borehole (Mazurek et al., 2023).Mazurek et al. (2023) demonstrated that, aside from hydraulically active fractures, diffusion remains the dominant transport mechanism even in the weathered Opalinus Clay encountered in the Lausen borehole.

The Amaltheenton Fm shows similarly high hydraulic conductivity values from field measurements, but extending to greater depths than reported for the OPA, with values up to 10^{-6} m/s at approximately 95 m depth. In contrast, laboratory measurements for both formations consistently fall below 10^{-12} m/s, aligning with the previously defined range of natural hydraulic conductivity variability for the intact rock matrix. However, *in situ* data from AMA borehole BO4 reveal a depth-dependent trend in hydraulic conductivity comparable to that observed in the OPA. In both formations, it is evident that the burial-induced matrix properties, reflected in small-scale hydraulic behaviour, are superimposed by on fracture-dominated advective flow at the field scale. However, the depth to which these matrix characteristics are overprinted by fracture-related permeability appears to differ substantially between formations.

Fracture formation in claystone at shallow depths is associated with various weathering and mechanical decompaction processes (Einsele et al., 1985; Hekel, 1994), including: (a) uplift and exhumation, which decrease vertical effective stress and promote volumetric expansion and fracturing, particularly along bedding planes; (b)

thermal expansion and contraction due to seasonal temperature fluctuations, typically affecting depths of up to ~30 m; and (c) de- and re-saturation cycles that increase suction and capillary pressures, leading to volumetric changes, fracturing, and disintegration. According to Hekel (1994), the depth variability of hydraulically conductive zones in the shallow Opalinus Clay of southern Germany is closely linked to topographic and geomorphological evolution. Elevated hydraulic conductivities in deeper borehole sections were mainly observed beneath older valleys (pre-Würm glaciation) and hill ridges, whereas the decompaction zone was less pronounced beneath younger valleys. The difference in the depth of the decompacted zone between northern Switzerland and southern Germany may reflect contrasting uplift and decompaction histories at ~~both~~ these sites (Vogt et al., 2017). This could likewise explain the greater depth of hydraulically active fractures observed in the AMA. Additionally, the local tectonic framework must be considered as a potential source of fracturing (e.g., due to nearby fault systems). Moreover, the swelling of clay minerals contributes to volumetric expansion by drawing in free water into the material. The magnitude of this volume increase depends on the degree of confinement, being substantially greater under unconfined than in confined conditions (Bock et al., 2010). Zhang (2010) demonstrated that unconfined swelling can result in volume expansions of up to 8 – 12 %, significantly contributing to decompaction. Under confined conditions, swelling leads instead to the buildup of swelling pressures acting against the surrounding material (Bock et al., 2010). Although most studies report swelling pressures ≤1 MPa, several have shown that moderately indurated claystone can develop pressures of 3 – 10 MPa, depending on clay mineral composition and effective confinement (Zhang, 2010; Wang et al., 2022). The reduction of vertical confinement due to uplift and exhumation can cause the dissipation of excess swelling pressure through vertical expansion and associated loss of cohesion, ultimately enhancing decompaction. Indeed, Mazurek et al. (2023) demonstrated that in the shallow OPA, significant porosity increases (up to nearly 40 %) occur as a result of the formations poor cementation and high content of swellable clay minerals.

5.3.2 Intact rock zone

~~Beyond~~ Below the decompaction zone, a consistent hydraulic regime appears to prevail in moderately indurated formations that have experienced burial depths of less than 2,000 m. In the context of this study, this includes the COx, the OPA, and those parts of the AMA encountered at borehole locations BO1 and BO2. Laboratory-derived hydraulic conductivity values for these formations collectively fall within the range of 10^{-14} to 10^{-12} m/s. For both the COx and OPA, *in situ* data obtained from similar depths lie within the same range. No depth-specific data are yet available for the AMA ~~beyond the decompaction~~for this zone. However, the present study has shown that, for the OPA and COx, laboratory measurements provide reliable representations of the rock mass hydraulic behaviour outside fault zones. This correspondence is primarily attributed to the efficient self-sealing capacity of both formations, which results from the combined effects of their clay mineral swelling potential and the effective stress conditions at depth (Bock et al., 2010; Di Donna et al., 2022; Voltolini and Ajo-Franklin, 2020; Berry et al., 2025).

5.4 Scope and limitations of the compiled dataset

The dataset compiled for this meta study integrates hydraulic, petrophysical, mineralogical, and burial history data from six argillaceous formations, spanning laboratory and field scales. While this data allows systematic links between burial evolution and hydraulic behaviour to be drawn across formations, it also introduces several sources of heterogeneity that should be considered when interpreting the results.

Formatiert: Schriftart: Kursiv

Formatiert: Überschrift 2, Abstand Vor: 0 Pt., Nach: 12 Pt.

Formatiert: Abstand Vor: 0 Pt., Nach: 0 Pt.

First, the compiled data originate from a wide range of studies conducted over several decades, employing different testing methods, test conditions, and sampling protocols. While we account for this variability through careful review of the included references, such heterogeneity introduces potential bias that cannot be fully excluded. For example, sample orientation with respect to bedding is not reported for all laboratory measurements. Although, the anisotropy observed in this study is comparatively low (K_p/K_s = ~1.1 to 2.7), studies suggest that the anisotropy ratio can yield values up to 5 or even exceeding these (Clennell et al., 1999; Bastiaens et al., 2007; Bock, 202; Neuzil, 2019). Such methodological differences represent an additional, largely unquantifiable source of scatter contributing to the natural variability envelope defined in section 4.3.4.

Second, argillaceous formations are internally heterogeneous at the facies scale (e.g., variations in carbonate type and content, grain size distribution, or bedding structure within a single formation), which cannot be fully resolved in the present compilation. Moreover, the properties reported here were measured at specific boreholes or sampling locations and may not be representative of the same formation elsewhere. Formations of broadly similar lithological composition and depositional origin will exhibit exactly the same hydraulic behaviour. Thus, the trends identified in this study should not be extrapolated to other formations or occurrences without independent verification. The formation-averaged hydraulic behaviour discussed here may therefore mask internal variability that is relevant at the scale of a specific repository site.

Third, the reconstruction of maximum burial depth for each formation carries formation-specific uncertainty. Burial estimates were adopted from published reconstructions rather than independently determined, and rely on different methods depending on data availability (e.g., basin modelling, vitrinite reflectance, apatite fission track analysis), which are not equally well constrained across all six formations. For example, for To-Do, the Clay Club Catalogue reports 1,300 – 1,700 metres of maximum burial, while other references (e.g., Mazurek et al. 2008, 2011), report approximately 2,000 m. For the AMA in the Hils syncline, the maturity trend is very well established (Littke et al., 1988; Burchartz et al., 2026), but calculated maximum temperatures and maximum burial depths vary, depending on i) basal heat flow, ii) selected lithologies of eroded sediments, and iii) the algorithm describing the kinetics of vitrinite reflectance increase (Bruns et al., 2016; Froidl et al., 2020).

Fourth, the number of available measurements differs substantially between formations and analyses. For formations that faced maximum burial >2,000 m, little hydraulic data is publically available, constraining derived analysis to few measurements or data ranges. The trends identified for these categories should be regarded as indicative rather than conclusively established. Additionally, data from maximum burial depths <850 m is represented by a single formation (Boom Clay).

Addressing these gaps, through additional first-hand data from underrepresented depth ranges and formations, and more systematic reporting of pore structure and mineralogy across future studies, remains an important direction for future work.

5.54 Summary and Synthesis

Formatiert: Abstand Vor: 12 Pt., Nach: 0 Pt.

Formatiert: Tiefgestellt

Formatiert: Tiefgestellt

The compiled and discussed data indicate that maximum burial depth, and the associated stress and temperature history, emerge as a primary and consistent control of hydraulic conductivity across the investigated formations. Together with mineralogical composition, and spatial mineral and pore-size distribution, these burial-related processes govern the spatial and temporal evolution of hydraulic conductivity in argillaceous formations. ~~The compiled and discussed data demonstrates that the burial history and associated stress and temperature conditions, together with mineralogical composition, exerts a primary control on the spatial and temporal hydraulic conductivity of argillaceous formations. Some key conclusions can be drawn or confirmed from the observations made:~~

Fluid flow through consolidated, stiff clay formations such as Boom Clay, and slightly to moderately indurated argillaceous rocks (COx, OPA) can be adequately described by means of classical continuum concepts, representing the material as porous media (Bock et al., 2010). In these cases, where formations remain unaffected by weathering and decompaction, the matrix hydraulic conductivity is representative of upscaled rock mass properties. ~~On~~ At both scales, diffusion can therefore be considered the dominant solute transport mechanism. In contrast, highly and very highly indurated and brittle formations show increasing influence of fracture flow. ~~,~~ so that ~~Consequently,~~ matrix and rock mass hydraulic conductivity diverge as advective processes dominate the hydraulic behaviour on a rock mass scale. In such cases, discrete fracture network approaches (such as done by Tóth et al.~~,~~ ~~(2022,~~ (2022) for BCF) provide a more meaningful framework for understanding fluid flow and solute transport processes within these formations (Bock et al. 2010).

6 Conclusion and Outlook

Predicting hydraulic conductivity and its potentially transient behaviour in argillaceous formations remains a fundamental and challenging task in the evaluation of potential host rocks for HLW. In such formations, fluid flow is governed by a complex interplay of compositional characteristics (e.g., mineralogy~~, grain size distribution~~, microstructure such as grain and pore size distribution) and diagenetic factors (stress and temperature history, present-day and palaeo-depth), which together shape the hydraulic properties across spatial and temporal scales.

This study compiled and analyzed hydraulic conductivity data from laboratory and field experiments in six argillaceous formations considered for HLW disposal in Europe. Together, the studied formations represent a paragenetic sequence that spans from the early diagenetic, moderately compacted, stiff Boom Clay (eodiagenesis), over mid-diagenetic claystones (mesodiagenesis) such COx, and OPA, to late-diagenetic, deeply buried, highly indurated, and brittle claystones (e.g., Boda Claystone Formation). Formations of the two latter groups have undergone (partly) significant uplift subsequent to maximum burial and thus exhibit pronounced but variable over-consolidation. The data highlights the complex interplay between intrinsic material properties and post-depositional geological processes that cover both, the burial up to maximum depth and the uplift to the present-day depth.

The Boom Clay represents the shallow burial end-member of the compiled data. At comparably low compaction, the hydraulic conductivity appears to be dependent on the stratigraphic zonation and associated compositional heterogeneity, rather than on present-day depth variability, as only a minor depth trend in a range between 56 m

to 365 m is apparent. However, the degree of compaction associated with variable burial still results in reduced porosity and associated hydraulic conductivity reduction.

Formations that experienced deeper burial (850 – 2,000 m) display a more complex pattern. They were subject to enhanced compaction and cementation processes and show a dependency to both present-day and maximum burial depths. The vast majority of hydraulic conductivities obtained from laboratory experiments falls into a narrow range between 10^{-14} to 10^{-12} m/s. This range is associated with a natural variability potentially as a result to of compositional differences between the investigated formations, sampling bias, bedding anisotropy between the tested samples, or methodological factors (e.g., applied stress; cf. Crisci et al., 2019). The results indicate that lab hydraulic conductivity is strongly linked to matrix characteristics imposed during maximum burial (e.g., porosity and void ratio reduction) and remains largely unaffected by subsequent uplift processes, provided weathering is absent. The bulk hydraulic behaviour as assessed based on *in situ* experiments shows a distinctively different behaviour. A clear present day depth dependency is evident from the compiled *in situ* data, showing strongly enhanced hydraulic conductivity in the upper 100 m and an exponential decay with depth. This trend is associated with the development of a pronounced decompaction zone as consequence to unloading effects and swelling pressures exceeding vertical effective stress conditions. However, in deeper sections *in situ* and laboratory data converge indicating efficient self-sealing processes with respect to fractures. In this zone matrix K as derived from laboratory experiments is indicative of rock mass characteristics, considering the natural variability range of 1 to 2 orders of magnitude.

From burial depths >2,000 m, a divergence between laboratory and *in situ* derived hydraulic conductivity becomes apparent, i.e., hydraulic conductivity on the field scale can be several orders of magnitude higher than matrix permeability measured on smaller, fracture-free samples in the lab.

The Boda Claystone Formation represents the deep burial end-member, having reached depths of up to 4,500 m. Such extreme burial has left a lasting imprint on the rock's petrophysical, mineralogical, mechanical, and hydraulic characteristics. The formation is highly indurated, brittle, and exhibits very low porosity. At the matrix scale, hydraulic conductivity derived from laboratory permeameter experiments is predictably low, ranging between 10^{-14} and 10^{-13} m/s. In contrast, at the rock-mass scale, hydraulic behaviour is dominated by open fractures, which persist due to the brittle nature of the rock that promotes fracturing during uplift and stress release. The limited presence of swellable clay minerals, likely a consequence of smectite-to-illite conversion at high burial temperatures, further prevents effective self-sealing of these fractures. As a result, field-based measurements of hydraulic conductivity span several orders of magnitude, reflecting the heterogeneity and dominance of unsealed fracture networks in controlling bulk flow.

While this study highlights consistent depth-related patterns, uncertainties remain due to sampling bias, site-specific differences, and methodological variability. However, the clear relationships between maximum burial, present-day depth, and hydraulic behaviour demonstrate that the long-term performance of argillaceous host rocks cannot be evaluated without considering geological history. Predictive models for repository safety must therefore integrate these evolutionary controls to assess the future behaviour of both matrix and rock mass hydraulic properties.

Formatiert: Rahmen: Rechts: (Kein Rahmen)

7. Appendices

Table A 1 Summary of literature sources for the compiled dataset

Formation	***Data reference***
Boom Clay	(Horseman et al., 1987; Bastiaens et al., 2007; Aertsens et al., 2008; Wemaere et al., 2008; Deng et al., 2011; Maes et al., 2011; Yu et al., 2011; Honty and De Craen, 2012; Aertsens et al., 2013; Hemes et al., 2013; Zeelmaekers et al., 2015; Frederickx et al., 2018; Jacops et al., 2020; Frederickx et al., 2021; Durce et al., 2024)
Amaltheenton Formation	(Burchartz et al., 2026)
Toarcian-Domerian Argillite	(Boisson et al., 2001; Patriarche et al., 2004b; Humbezi Desfeux et al., 2024)
Callovo-Oxfordian Argillite	(Gaucher et al., 2004; Delay et al., 2006; Distinguin and Lavanchy, 2007; Yven et al., 2007; Wan et al., 2013; Hu et al., 2014; Jacops and Maes, 2015; Belmokhtar et al., 2017; Song et al., 2017; Wang et al., 2022b)
Opalinus Clay	(Hekel, 1994; Croisé et al., 2004; Wersin et al., 2013; Vogt et al., 2017; Yu et al., 2017; Mazurek et al., 2023) Nagra work reports: accessible via https://nagra.ch/en/downloads-2/)
Boda Claystone Formation	(Fedor et al., 2008, 2019; OECD and NEA, 2022; Lázár et al., 2024)

Data availability. All data are~~is~~ publically available from the references listed in table A1 or presented in this paper.

Author contribution. RB, BMM, GG, MRJ, RL, FA: investigation. RB, RL: writing (original draft preparation). RB: visualization. RB, BMM, PAZ, TS, LW, GG, YS, MRJ, RL, FA: writing (review & editing). FA, RL: conceptualization, funding acquisition. FA, RL, YS: supervision.

Competing interests. The authors declare that they have no conflict of interest.

Acknowledgements. The MATURITY project received funding from the Federal Company for Radioactive Waste Disposal and the Federal Ministry for Economic Affairs and Climate Action, which is greatly acknowledged. We would like to sincerely thank all three anonymous reviewers for their excellent and constructive work, which has significantly helped to improve our manuscript. We would also like to thank Dr. Sylvie Demouchy for her great editorial work.

References

Addis, M. A. and Jones, M. E.: Volume changes during diagenesis, Marine and Petroleum Geology, 2, 241–246, https://doi.org/10.1016/0264-8172(85)90013-3, 1985.

Aertsens, M., Put, M., and Dierckx, A.: An analytical model for the interpretation of pulse injection experiments performed for testing the spatial variability of clay formations, Journal of Contaminant Hydrology, 61, 423–436, https://doi.org/10.1016/S0169-7722(02)00118-3, 2003.

Aertsens, M., Wemaere, I., and Wouters, L.: Spatial variability of transport parameters in the Boom Clay, Applied Clay Science, 26, 37–45, https://doi.org/10.1016/j.clay.2003.09.015, 2004.

Aertsens, M., Van Gompel, M., De Cannière, P., Maes, N., and Dierckx, A.: Vertical distribution of transport parameters in Boom Clay in the Mol-1 borehole (Mol, Belgium), Physics and Chemistry of the Earth, Parts A/B/C, 33, S61–S66, https://doi.org/10.1016/j.pce.2008.10.060, 2008.

Aertsens, M., Maes, N., Labat, S., Van Gompel, M., and Maes, T.: Vertical distribution of HTO and 125I− transport parameters in Boom Clay in the Essen-1 borehole (Mol, Belgium), Physics and Chemistry of the Earth, Parts A/B/C, 65, 90–97, https://doi.org/10.1016/j.pce.2013.05.006, 2013.

Appel, D. and Habler, W.: Quantifizierung der Wasserdurchlässigkeit von Gesteinen als Voraussetzung für die Entwicklung von Kriterien zur Grundwasserbewegung - Phase 1: Überprüfung der Datenbasis für die Ableitung von Kriterien zur Wasserdurchlässigkeit, Arbeitskreis Auswahlverfahren Endlagerstandorte, 2001.

Árkai, P., Balogh, K., Demeny, A., Nagy, G., and Mathe, Z.: Composition, diagenetic and post-diagenetic alterations of a possible radioactive waste repository site: the Boda Albitic Claystone Formation, southern Hungary, 43, Acta Geologica Hungarica, Budapest, https://inis.iaea.org/records/y75zw-0rx55, 2000.

Asem, P. and Gardoni, P.: A probabilistic, empirical model for permeability of mudstone, Probabilistic Engineering Mechanics, 69, 103262, https://doi.org/10.1016/j.probengmech.2022.103262, 2022.

Athy, L. F.: Density, Porosity and Compaction of Sedimentary Rocks, Bulletin of the American Association of Petroleum Geologists (AAPG Bulletin), 14, 1–24, https://doi.org/10.1306/3D93289E-16B1-11D7-8645000102C1865D, 1930.

Avseth, P., Mavko, G., Dvorkin, J., and Mukerji, T.: Rock physics and seismic properties of sands and shales as a function of burial depth, in: SEG Technical Program Expanded Abstracts 2001, SEG Technical Program Expanded Abstracts 2001, 1780–1783, https://doi.org/10.1190/1.1816471, 2001.

Barbarand, J., Lucazeau, F., Pagel, M., and Séranne, M.: Burial and exhumation history of the south-eastern Massif Central (France) constrained by apatite fission-track thermochronology, Tectonophysics, 335, 275–290, https://doi.org/10.1016/S0040-1951(01)00069-5, 2001.

Bastiaens, W., Bernier, F., and Li, X. L.: SELFRAC: Experiments and conclusions on fracturing, self-healing and self-sealing processes in clays, Physics and Chemistry of the Earth, Parts A/B/C, 32, 600–615, https://doi.org/10.1016/j.pce.2006.04.026, 2007.

Batlle-Aguilar, J., Cook, P. G., and Harrington, G. A.: Comparison of hydraulic and chemical methods for determining hydraulic conductivity and leakage rates in argillaceous aquitards, Journal of Hydrology, 532, 102–121, https://doi.org/10.1016/j.jhydrol.2015.11.035, 2016.

Beaucaire, C., Michelot, J.-L., Savoye, S., and Cabrera, J.: Groundwater characterisation and modelling of water–rock interaction in an argillaceous formation (Tournemire, France), Applied Geochemistry, 23, 2182–2197, https://doi.org/10.1016/j.apgeochem.2008.03.003, 2008.

Belmokhtar, M., Delage, P., Ghabezloo, S., Tang, A.-M., Menaceur, H., and Conil, N.: Poroelasticity of the Callovo–Oxfordian Claystone, Rock Mech Rock Eng, 50, 871–889, https://doi.org/10.1007/s00603-016-1137-3, 2017.

Berry, T., Murphy, W., and Paraskevopoulou, C.: Self-sealing of argillaceous media in the context of geological disposal of radioactive waste – a perspective from past and ongoing studies, Geoenergy, 3, geoenergy2024-021, https://doi.org/10.1144/geoenergy2024-021, 2025.

Berthonneau, J., Hoover, C. G., Grauby, O., Baronnet, A., Pellenq, R. J.-M., and Ulm, F.-J.: Crystal-chemistry control of the mechanical properties of 2:1 clay minerals, Applied Clay Science, 143, 387–398, https://doi.org/10.1016/j.clay.2017.04.010, 2017.

Bjørlykke, K.: Principal aspects of compaction and fluid flow in mudstones, in: Muds and Mudstones. Physical and Fluid FlowProperties, vol. 158, The Geological Society of London, London, 73–78, https://doi.org/https://doi.org/10.1144/gsl.sp.1999.158.01.06, 1999.

Bjørlykke, K.: Relationships between depositional environments, burial history and rock properties. Some principal aspects of diagenetic process in sedimentary basins, Sedimentary Geology, 301, 1–14, https://doi.org/10.1016/j.sedgeo.2013.12.002, 2014.

Bjørlykke, K. and Høeg, K.: Effects of burial diagenesis on stresses, compaction and fluid flow in sedimentary basins, Marine and Petroleum Geology, 14, 267–276, https://doi.org/10.1016/S0264-8172(96)00051-7, 1997.

Blaise, T., Barbarand, J., Kars, M., Ploquin, F., Aubourg, C., Brigaud, B., Cathelineau, M., El Albani, A., Gautheron, C., Izart, A., Janots, D., Michels, R., Pagel, M., Pozzi, J.-P., Boiron, M.-C., and Landrein, P.: Reconstruction of low temperature (<100 °C) burial in sedimentary basins: A comparison of geothermometer in the intracontinental Paris Basin, Marine and Petroleum Geology, 53, 71–87, https://doi.org/10.1016/j.marpetgeo.2013.08.019, 2014.

Bock, H., Dehandschutter, B., Martin, D. C., Haller, A. de, Mazurek, M., Skoczylas, F., and Davy, C. (Eds.): Self-sealing of fractures in argillaqceous formations in the context of geological disposal of radioactive waste: review and synthesis, NEA No. 6184, OECD, Paris, https://www.oecd-nea.org/jcms/pl_14208/self-sealing-of-fractures-in-argillaceous-formations-in-the-context-of-geological-disposal-of-radioactive-waste?details=true, 2010.

Boisson, J.-Y., Bertrand, L., Heitz, J.-F., and Golvan, Y.: In situ and laboratory investigations of fluid flow through an argillaceous formation at different scales of space and time, Tournemire tunnel, southern France, Hydrogeology Journal, 9, 108–123, https://doi.org/10.1007/s100400000119, 2001.

Bonin, B.: Deep geological disposal in argillaceous formations: studies at the Tournemire test site, Journal of Contaminant Hydrology, 35, 315–330, https://doi.org/10.1016/S0169-7722(98)00132-6, 1998.

Bowers, G. L.: Pore Pressure Estimation From Velocity Data: Accounting for Overpressure Mechanisms Besides Undercompaction, SPE Drilling & Completion, 10, 89–95, https://doi.org/10.2118/27488-PA, 1995.

Bredehoeft, J. D. and Papadopulos, S. S.: A method for determining the hydraulic properties of tight formations, Water Resources Research, 16, 233–238, https://doi.org/10.1029/WR016i001p00233, 1980.

Bruns, B., Littke, R., Gasparik, M., Van Wees, J. -D., and Nelskamp, S.: Thermal evolution and shale gas potential estimation of the Wealden and Posidonia Shale in NW -Germany and the Netherlands: a 3D basin modelling study, Basin Research, 28, 2–33, https://doi.org/10.1111/bre.12096, 2016.

Burchartz, R., Seemann, T., Gaus, G., Winhausen, L., Jalali, M., Mbui, B. M., Grohmann, S., Burnaz, L., Colling Cassel, M., Erbacher, J., Littke, R., and Amann, F.: The influence of burial history on physical rock properties: a case study of Lower Jurassic claystones from the Hils and Sack Synclines (Germany), Solid Earth, 17, 485–512, https://doi.org/10.5194/se-17-485-2026, 2026.

Burnaz, L., Littke, R., Grohmann, S., Erbacher, J., Strauss, H., and Amann, F.: Lower Jurassic (Pliensbachian–Toarcian) marine paleoenvironment in Western Europe: sedimentology, geochemistry and organic petrology of the wells Mainzholzen and Wickensen, Hils Syncline, Lower Saxony Basin, Int J Earth Sci (Geol Rundsch), https://doi.org/10.1007/s00531-023-02381-8, 2024.

Carcione, J. M., Gei, D., Yu, T., and Ba, J.: Effect of Clay and Mineralogy on Permeability, Pure Appl. Geophys., 176, 2581–2594, https://doi.org/10.1007/s00024-019-02117-3, 2019.

Carcione, J. M., Gei, D., Picotti, S., Qadrouh, A. N., Alajmi, M., and Ba, J.: Rock Acoustics of Diagenesis and Cementation, Pure Appl. Geophys., 179, 1919–1934, https://doi.org/10.1007/s00024-022-03016-w, 2022.

Castro-Vera, L., Amberg, S., Gaus, G., Leu, K., and Littke, R.: 3D basin modeling of the Hils Syncline, Germany: reconstruction of burial and thermal history and implications for petrophysical properties of potential Mesozoic shale host rocks for nuclear waste storage, Int J Earth Sci (Geol Rundsch), https://doi.org/10.1007/s00531-024-02384-z, 2024.

Charpentier, D., Tessier, D., and Cathelineau, M.: Shale microstructure evolution due to tunnel excavation after 100 years and impact of tectonic paleo-fracturing. Case of Tournemire, France, Engineering Geology, 70, 55–69, https://doi.org/10.1016/S0013-7952(03)00082-6, 2003.

Clennell, M. B., Dewhurst, D. N., Brown, K. M., and Westbrook, G. K.: Permeability anisotropy of consolidated clays, SP, 158, 79–96, https://doi.org/10.1144/GSL.SP.1999.158.01.07, 1999.

Constantin, J., Vergély, P., and Cabrera, J.: Tectonic evolution and related fracturing in the Causses Basin (Aveyron, France) : the Tournemire area example, Bulletin de la Société Géologique de France, 173, 229–243, https://doi.org/10.2113/173.3.229, 2002.

Constantin, J., Peyaud, J. B., Vergély, P., Pagel, M., and Cabrera, J.: Evolution of the structural fault permeability in argillaceous rocks in a polyphased tectonic context, Physics and Chemistry of the Earth, Parts A/B/C, 29, 25–41, https://doi.org/10.1016/j.pce.2003.11.001, 2004.

Cosenza, P., Robinet, J. C., Prêt, D., Huret, E., Fleury, M., Géraud, Y., Lebon, P., Villiéras, F., and Zamora, M.: Indirect estimation of the clay content of clay-rocks using acoustic measurements: New insights from the Montiers-sur-Saulx deep borehole (Meuse, France), Marine and Petroleum Geology, 53, 117–132, https://doi.org/10.1016/j.marpetgeo.2013.07.004, 2014.

Cripps, J. C. and Czerewko, M. A.: The influence of diagenetic and mineralogical factors on the breakdown and geotechnical properties of mudrocks, Geological Society, London, Special Publications, 454, 271–293, https://doi.org/10.1144/SP454.10, 2017.

Crisci, E., Ferrari, A., Giger, S. B., and Laloui, L.: Hydro-mechanical behaviour of shallow Opalinus Clay shale, Engineering Geology, 251, 214–227, https://doi.org/10.1016/j.enggeo.2019.01.016, 2019.

Croisé, J., Schlickenrieder, L., Marschall, P., Boisson, J. Y., Vogel, P., and Yamamoto, S.: Hydrogeological investigations in a low permeability claystone formation: the Mont Terri Rock Laboratory, Physics and Chemistry of the Earth, Parts A/B/C, 29, 3–15, https://doi.org/10.1016/j.pce.2003.11.008, 2004.

Czerewko, M. A. and Cripps, J. C.: The implications of diagenetic history and weathering on the engineering behaviour of mudrocks, 10th Congress of the International Association for Engineering Geology and the Environment, 118, The Geological Society of London, Nottingham, UK, https://media.geolsoc.org.uk/iaeg2006/INDEXES/HOME.HTM (last access: 13 January 2025), 2006.

De Windt, L., Cabrera, J., and Boisson, J. Y.: Radioactive waste containment in indurated shales: comparison between the chemical containment properties of matrix and fractures, SP, 157, 167–181, https://doi.org/10.1144/GSL.SP.1999.157.01.13, 1999.

Dehandschutter, B., Vandycke, S., Sintubin, M., Vandenberghe, N., and Wouters, L.: Brittle fractures and ductile shear bands in argillaceous sediments: inferences from Oligocene Boom Clay (Belgium), Journal of Structural Geology, 27, 1095–1112, https://doi.org/10.1016/j.jsg.2004.08.014, 2005.

Delage, P., Cui, Y. J., and Tang, A. M.: Clays in radioactive waste disposal, Journal of Rock Mechanics and Geotechnical Engineering, 2, 111–123, https://doi.org/10.3724/SP.J.1235.2010.00111, 2010.

Delay, J., Trouiller, A., and Lavanchy, J.-M.: Propriétés hydrodynamiques du Callovo-Oxfordien dans l'Est du bassin de Paris : comparaison des résultats obtenus selon différentes approches, Comptes Rendus. Géoscience, 338, 892–907, https://doi.org/10.1016/j.crte.2006.07.009, 2006.

Delay, J., Distinguin, M., and Dewonck, S.: Characterization of a clay-rich rock through development and installation of specific hydrogeological and diffusion test equipment in deep boreholes, Physics and Chemistry of the Earth, Parts A/B/C, 32, 393–407, https://doi.org/10.1016/j.pce.2006.01.011, 2007.

Deng, Y.-F., Tang, A.-M., Cui, Y.-J., and Li, X.-L.: Study on the hydraulic conductivity of Boom clay, Can. Geotech. J., 48, 1461–1470, https://doi.org/10.1139/t11-048, 2011.

Dewhurst, D. N., Aplin, A. C., Sarda, J., and Yang, Y.: Compaction-driven evolution of porosity and permeability in natural mudstones: An experimental study, J. Geophys. Res., 103, 651–661, https://doi.org/10.1029/97JB02540, 1998.

Dewhurst, D. N., Aplin, A. C., and Sarda, J.: Influence of clay fraction on pore-scale properties and hydraulic conductivity of experimentally compacted mudstones, J. Geophys. Res., 104, 29261–29274, https://doi.org/10.1029/1999JB900276, 1999.

Di Donna, A., Charrier, P., Dijkstra, J., Andò, E., and Bésuelle, P.: The contribution of swelling to self-sealing of claystone studied through x-ray tomography, Physics and Chemistry of the Earth, Parts A/B/C, 127, 103191, https://doi.org/10.1016/j.pce.2022.103191, 2022.

Distinguin, M. and Lavanchy, J.-M.: Determination of hydraulic properties of the Callovo-Oxfordian argillite at the bure site: Synthesis of the results obtained in deep boreholes using several in situ investigation techniques, Physics and Chemistry of the Earth, Parts A/B/C, 32, 379–392, https://doi.org/10.1016/j.pce.2006.02.056, 2007.

Durce, D., Aertsens, M., Maes, N., Van Gompel, M., and Brassinnes, S.: Comparison of lab-scale experiments for the determination of non-reactive tracer diffusion coefficients in Boom Clay, Applied Geochemistry, 173, 106101, https://doi.org/10.1016/j.apgeochem.2024.106101, 2024.

Einsele, G., Heitfeld, K.-H., Lempp, Ch., and Schetelig, K.: Auflockerung und Verwitterung in der Ingenieurgeologie: Übersicht, Feldansprache, Klassifikation (Verwitterungsprofile) — Einleitender Beitrag, in: Ingenieurgeologische Probleme im Grenzbereich zwischen Locker- und Festgesteinen, edited by: Heitfeld, K.-H., Springer Berlin Heidelberg, Berlin, Heidelberg, 2–23, https://doi.org/10.1007/978-3-642-70452-9_1, 1985.

Esteban, L., Géraud, Y., and Bouchez, J. L.: Pore network connectivity anisotropy in Jurassic argillite specimens from eastern Paris Basin (France), Physics and Chemistry of the Earth, Parts A/B/C, 32, 161–169, https://doi.org/10.1016/j.pce.2005.11.001, 2007.

Ewy, R., Dirkzwager, J., and Bovberg, C.: Claystone porosity and mechanical behavior vs. geologic burial stress, Marine and Petroleum Geology, 121, 104563, https://doi.org/10.1016/j.marpetgeo.2020.104563, 2020.

Favero, V.: Multiphysical behaviour of shales from Northern Switzerland, Ph.D. thesis, EPFL, Lausanne, Switzerland, 279 pp., https://doi.org/https://doi.org/10.5075/epfl-thesis-7539, 2017.

Favero, V., Ferrari, A., and Laloui, L.: Anisotropic Behaviour of Opalinus Clay Through Consolidated and Drained Triaxial Testing in Saturated Conditions, Rock Mech Rock Eng, 51, 1305–1319, https://doi.org/10.1007/s00603-017-1398-5, 2018.

Fedor, F., Hámos, G., Jobbik, A., Máthé, Z., Somodi, G., and Szűcs, I.: Laboratory pressure pulse decay permeability measurement of Boda Claystone, Mecsek Mts., SW Hungary, Physics and Chemistry of the Earth, Parts A/B/C, 33, S45–S53, https://doi.org/10.1016/j.pce.2008.10.059, 2008.

Fedor, F., Máthé, Z., Ács, P., and Koroncz, P.: New results of Boda Claystone research: Genesis, mineralogy, geochemistry, petrophysics, Geological Society, London, Special Publications, 482, 75–92, https://doi.org/10.1144/SP482.13, 2019.

Ferrari, A., Favero, V., and Laloui, L.: One-dimensional compression and consolidation of shales, International Journal of Rock Mechanics and Mining Sciences, 88, 286–300, https://doi.org/10.1016/j.ijrmms.2016.07.030, 2016.

Ferris, D. M., Potter, G., and Ferguson, G.: Characterization of the hydraulic conductivity of glacial till aquitards, Hydrogeol J, 28, 1827–1839, https://doi.org/10.1007/s10040-020-02161-7, 2020.

Frederickx, L., Honty, M., De Craen, M., Dohrmann, R., and Elsen, J.: Relating the Cation Exchange Properties of the Boom Clay (Belgium) to Mineralogy and Pore-Water Chemistry, Clays and clay miner., 66, 449–465, https://doi.org/10.1346/CCMN.2018.064111, 2018.

Formatiert: Deutsch (Deutschland)

Frederickx, L., Honty, M., De Craen, M., and Elsen, J.: Evaluating the quantification of the clay mineralogy of the Rupelian Boom Clay in Belgium by a detailed study of size fractions, Applied Clay Science, 201, 105954, https://doi.org/10.1016/j.clay.2020.105954, 2021.

Froidl, F., Zieger, L., Mahlstedt, N., and Littke, R.: Comparison of single- and multi-ramp bulk kinetics for a natural maturity series of Westphalian coals: Implications for modelling petroleum generation, International Journal of Coal Geology, 219, 103378, https://doi.org/10.1016/j.coal.2019.103378, 2020.

Gale, J. F. W., Laubach, S. E., Olson, J. E., Eichhuble, P., and Fall, A.: Natural Fractures in shale: A review and new observations, AAPG Bulletin, 98, 2165–2216, https://doi.org/10.1306/08121413151, 2014.

Gaucher, E., Robelin, C., Matray, J. M., Négrel, G., Gros, Y., Heitz, J. F., Vinsot, A., Rebours, H., Cassagnabère, A., and Bouchet, A.: ANDRA underground research laboratory: interpretation of the mineralogical and geochemical data acquired in the Callovian–Oxfordian formation by investigative drilling, Physics and Chemistry of the Earth, Parts A/B/C, 29, 55–77, https://doi.org/10.1016/j.pce.2003.11.006, 2004.

Gaus, G., Hoyer, E.-M., Seemann, T., Fink, R., Amann, F., and Littke, R.: Laboratory investigation of permeability, pore space and unconfined compressive strength of uplifted Jurassic mudstones: The role of burial depth and thermal maturation, zdgg, 173, 469–489, https://doi.org/10.1127/zdgg/2022/0329, 2022.

Gautschi, A.: Hydrogeology of a fractured shale (Opalinus Clay): Implications for deep geological disposal of radioactive wastes, Hydrogeology Journal, 9, 97–107, https://doi.org/10.1007/s100400000117, 2001.

Gautschi, A.: Safety-relevant hydrogeological properties of the claystone barrier of a Swiss radioactive waste repository: An evaluation using multiple lines of evidence, Grundwasser, 22, 221–233, https://doi.org/10.1007/s00767-017-0364-1, 2017.

Geng, Z., Bonnelye, A., David, C., Dick, P., Wang, Y., and Schubnel, A.: Pressure Solution Compaction During Creep Deformation of Tournemire Shale: Implications for Temporal Sealing in Shales, JGR Solid Earth, 126, e2020JB021370, https://doi.org/10.1029/2020JB021370, 2021.

Giger, S. B., Ewy, R. T., Favero, V., Stankovic, R., and Keller, L. M.: Consolidated-undrained triaxial testing of Opalinus Clay: Results and method validation, Geomechanics for Energy and the Environment, 14, 16–28, https://doi.org/10.1016/j.gete.2018.01.003, 2018.

Gonzalez-Blanco, L., Romero, E., and Levasseur, S.: Self-Sealing of Boom Clay After Gas Transport, Rock Mech Rock Eng, 57, 4173–4189, https://doi.org/10.1007/s00603-023-03529-3, 2024.

Hart, B. S., Schieber, J., and Kalinec, J.: Clay diagenesis and overpressure development in Upper Cretaceous and Tertiary shales of South Texas, Marine and Petroleum Geology, 147, 105978, https://doi.org/10.1016/j.marpetgeo.2022.105978, 2023.

Hekel, U.: Hydrogeologische Erkundung toniger Festgesteine am Beispiel des Opalinustons (Unteres Aalenium), Universität Tübingen, Tübingen, Germany, https://publikationen.uni-tuebingen.de/xmlui/handle/10900/56824, 1994.

Hemes, S., Desbois, G., Urai, J. L., De Craen, M., and Honty, M.: Variations in the morphology of porosity in the Boom Clay Formation: insights from 2D high resolution BIB-SEM imaging and Mercury injection Porosimetry, Netherlands Journal of Geosciences, 92, 275–300, https://doi.org/10.1017/S0016774600000214, 2013.

Honty, M. and De Craen, M.: Boom Clay mineralogy – qualitative and quantitative aspects: Status Report 2011, SCK CEN Reports; No. ER-194, SCK-CEN, Mol, Belgium, https://researchportal.sckcen.be/en/publications/boom-clay-mineralogy-qualitative-and-quantitative-aspects/, 2012.

Horseman, S. T., Winter, M. G., and Entwistle, D. C.: Geotechnical characterization of boom clay in relation to the disposal of radioactive waste, EUR--10987, Commission of the European Communities, Luxembourg, https://inis.iaea.org/records/dh1h6-qtf70, 1987.

Formatiert: Deutsch (Deutschland)

Formatiert: Deutsch (Deutschland)

Horseman, S. T., Higgo, J. A., Harrington, J. F., and NEA (Eds.): Water, gas and solute movement through argillaceous media, Report CC-91/1, Organisation for Economic Co-Operation and Development, Paris (France), https://inis.iaea.org/records/vdc40-6j882, 1996.

Hu, D. W., Zhang, F., Shao, J. F., and Gatmiri, B.: Influences of Mineralogy and Water Content on the Mechanical Properties of Argillite, Rock Mech Rock Eng, 47, 157–166, https://doi.org/10.1007/s00603-013-0413-8, 2014.

Humbezi Desfeux, M., Marcoux, M., Matray, J.-M., Gorny, J., Schädle, P., and Pochet, G.: DIGIT: An In Situ Experiment for Studying the Diffusion of Water and Solutes under Thermal Gradient in the Toarcian Clay Rock at the Tournemire Underground Research Laboratory: Part 1—Goals, Scoping Calculations, Installation and First Results under Unheated Conditions, Minerals, 14, 563, https://doi.org/10.3390/min14060563, 2024.

Ishii, E., Sanada, H., Funaki, H., Sugita, Y., and Kurikami, H.: The relationships among brittleness, deformation behavior, and transport properties in mudstones: An example from the Horonobe Underground Research Laboratory, Japan, J. Geophys. Res., 116, B09206, https://doi.org/10.1029/2011JB008279, 2011.

Jacops, E. and Maes, N.: Measuring the diffusion coefficient for He and Ar in Callovo-Oxfordian Clay, Final report, SCK-CEN-ER-301, SCK-CEN, Mol, Belgium, https://researchportal.sckcen.be/en/publications/measuring-the-diffusion-coefficient-for-he-and-ar-in-callovo-oxfo/, 2015.

Jacops, E., Rogiers, B., Frederickx, L., Swennen, R., Littke, R., Krooss, B. M., Amann-Hildenbrand, A., and Bruggeman, C.: The relation between petrophysical and transport properties of the Boom Clay and Eigenbilzen Sands, Applied Geochemistry, 114, 104527, https://doi.org/10.1016/j.apgeochem.2020.104527, 2020.

Jones, M. E. and Addis, M. A.: On changes in porosity and volume during burial of argillaceous sediments, Marine and Petroleum Geology, 2, 247–253, https://doi.org/10.1016/0264-8172(85)90014-5, 1985.

Kiczka, M., Wersin, P., Mazurek, M., Zwahlen, C., Jenni, A., Mäder, U., and Traber, D.: Porewater composition in clay rocks explored by advective displacement and squeezing experiments, Applied Geochemistry, 159, 105838, https://doi.org/10.1016/j.apgeochem.2023.105838, 2023.

Kneuker, T., Dohrmann, R., Ufer, K., and Jaeggi, D.: Compositional-structural characterization of the Opalinus Clay and Passwang Formation: New insights from Rietveld refinement (Mont Terri URL, Switzerland), Applied Clay Science, 242, 107017, https://doi.org/10.1016/j.clay.2023.107017, 2023.

Kneuker, T., Mann, T., Dohrmann, R., Ufer, K., Blumenberg, M., Erbacher, J., Bornemann, A., Schuck, B., Zimmerli, G. N., and Pollok, L.: Compositional-structural properties of the Opalinus Clay in southern Germany: Combining facies-based studies and mineralogical analyses, Applied Clay Science, 279, 108032, https://doi.org/10.1016/j.clay.2025.108032, 2026.

Konrád, G., Sebe, K., Halász, A., and Babinszki, E.: Sedimentology of a Permian playa lake: the Boda Claystone Formation, Hungary, Geologos, 16, https://doi.org/10.2478/v10118-010-0002-1, 2010.

Kovács, L.: Partial Self-Healing Effects of a Highly Indurated Claystone Formation (BCF) Discovered by In Situ Measurements, IGSC Working Group on Measurement and Physical Understanding of Groundwater Flow through Argillaceous Media (Clay Club) Self-Healing Topical Session Proceedings, NEA, Nancy, France, https://inis.iaea.org/records/hzg2z-87n09, 2001.

Laubach, S. E., Olson, J. E., and Gross, M. R.: Mechanical and fracture stratigraphy, AAPG Bulletin, 93, 1413–1426, https://doi.org/10.1306/07270909094, 2009.

Lázár, K., Máthé, Z., Németh, T., Kovács-Kis, V., Stichleutner, S., and Kovács, I.: Iron-Bearing Minerals in the Boda Claystone Formation: Correspondences with Stages of Evolution Revealed by Mössbauer Spectroscopy, Minerals, 14, 196, https://doi.org/10.3390/min14020196, 2024.

Littke, R., Baker, D. R., and Leythaeuser, D.: Microscopic and sedimentologic evidence for the generation and migration of hydrocarbons in Toarcian source rocks of different maturities, Advances in Organic Geochemistry, Vol.13, 549–559, https://doi.org/https://doi.org/10.1016/0146-6380(88)90075-7, 1988.

Mäder, U.: Advective Displacement Method for the Characterisation of Pore Water Chemistry and Transport Properties in Claystone, Geofluids, 2018, 1–11, https://doi.org/10.1155/2018/8198762, 2018.

Maes, N., Bruggeman, C., Govaerts, J., Martens, E., Salah, S., and Van Gompel, M.: A consistent phenomenological model for natural organic matter linked migration of Tc(IV), Cm(III), Np(IV), Pu(III/IV) and Pa(V) in the Boom Clay, Physics and Chemistry of the Earth, Parts A/B/C, 36, 1590–1599, https://doi.org/10.1016/j.pce.2011.10.003, 2011.

Marten, T., Ruebsam, W., Mutterlose, J., Wiesenberg, G. L. B., and Schwark, L.: Latest Pliensbachian to Early Toarcian depositional environment and organo-facies evolution in the North-German Basin (Hondelage Section), Int J Earth Sci (Geol Rundsch), https://doi.org/10.1007/s00531-024-02433-7, 2024.

Mazurek, M., Hurford, A. J., and Leu, W.: Unravelling the multi-stage burial history of the Swiss Molasse Basin: Integration of apatite fission track, vitrinite reflectance and biomarker isomerisation analysis., Basin Research, 18, 27–50, https://doi.org/https://doi.org/10.1111/j.1365-2117.2006.00286.x, 2006.

Mazurek, M., Gautschi, A., Marschall, P., Vigneron, G., Lebon, P., and Delay, J.: Transferability of geoscientific information from various sources (study sites, underground rock laboratories, natural analogues) to support safety cases for radioactive waste repositories in argillaceous formations, Physics and Chemistry of the Earth, Parts A/B/C, 33, S95–S105, https://doi.org/10.1016/j.pce.2008.10.046, 2008.

Mazurek, M., Alt-Epping, P., Bath, A., Gimmi, T., and Waber, H. N.: Natural Tracer Profiles Across Argillaceous Formations: The CLAYTRAC Project, OECD/NEA, Paris, https://doi.org/https://doi.org/10.1787/9789264060487-en, 2009.

Mazurek, M., Alt-Epping, P., Bath, A., Gimmi, T., Niklaus Waber, H., Buschaert, S., Cannière, P. D., Craen, M. D., Gautschi, A., Savoye, S., Vinsot, A., Wemaere, I., and Wouters, L.: Natural tracer profiles across argillaceous formations, Applied Geochemistry, 26, 1035–1064, https://doi.org/10.1016/j.apgeochem.2011.03.124, 2011.

Mazurek, M., Wersin, P., Hadi, J., Grenèche, J.-M., Prinpreecha, N., and Traber, D.: Geochemistry and palaeo-hydrogeology of the weathered zone in the Opalinus Clay, Applied Clay Science, 232, 106793, https://doi.org/10.1016/j.clay.2022.106793, 2023.

Mbui, B. M., Gaus, G., Littke, R., and Amann, F.: A Rapid Laboratory Method for Matrix-Scale Permeability Characterisation in Tight Rocks, Transp Porous Med, 153, 86, https://doi.org/10.1007/s11242-026-02332-2, 2026.

Menaceur, H., Delage, P., Tang, A.-M., and Conil, N.: The thermo-mechanical behaviour of the Callovo-Oxfordian claystone, International Journal of Rock Mechanics and Mining Sciences, 78, 290–303, https://doi.org/10.1016/j.ijrmms.2015.07.002, 2015.

Mertens, J., Vandenberghe, N., Wouters, L., and Sintubin, M.: The origin and development of joints in the Boom Clay Formation (Rupelian) in Belgium, SP, 216, 309–321, https://doi.org/10.1144/GSL.SP.2003.216.01.20, 2003.

Nagra: Synthese der geowissenschaftlichen Untersuchungsergebnisse, Nagra Technischer Bericht, NTB 02-03, Nagra, Wettingen, https://www.nagra.ch/reports/technischer-bericht-ntb-02-03, 2002.

Nagra: SGT-E3 deep drilling campaign (TBO): Experiment Procedures and Analytical Methods at RWI, University of Bern, Arbeitsbericht, NAB 20-13, Nagra, Wettingen, https://www.nagra.ch/reports/arbeitsbericht-nab-20-13, 2020.

Németh, T., Máthé, Z., Pekker, P., Dódony, I., Kovács-Kis, V., Sipos, P., Cora, I., and Kovács, I.: Clay mineralogy of the Boda Claystone Formation (Mecsek Mts., SW Hungary), Open Geosciences, 8, https://doi.org/10.1515/geo-2016-0024, 2016.

Neuzil, C. E.: How permeable are clays and shales?, Water Resources Research, 30, 145–150, https://doi.org/10.1029/93WR02930, 1994.

Neuzil, C. E.: Interpreting fluid pressure anomalies in shallow intraplate argillaceous formations, Geophysical Research Letters, 42, 4801–4808, https://doi.org/10.1002/2015GL064140, 2015.

Formatiert: Deutsch (Deutschland)

Neuzil, C. E.: Permeability of Clays and Shales, Annu. Rev. Earth Planet. Sci., 47, 247–273, https://doi.org/10.1146/annurev-earth-053018-060437, 2019.

Norris, S.: Radioactive waste confinement: clays in natural and engineered barriers – introduction, SP, 443, 1–8, https://doi.org/10.1144/SP443.26, 2017.

OECD and NEA: Clay Club Catalogue of Characteristics of Argillaceous Rocks: 2022 Update, OECD, https://doi.org/10.1787/8860f7d8-en, 2022.

Patriarche, D., Ledoux, E., Simon-Coinçon, R., Michelot, J.-L., and Cabrera, J.: Characterization and modeling of diffusion process for mass transport through the Tournemire argillites (Aveyron, France), Applied Clay Science, 26, 109–122, https://doi.org/10.1016/j.clay.2003.10.005, 2004a.

Patriarche, D., Ledoux, E., Michelot, J., Simon-Coinçon, R., and Savoye, S.: Diffusion as the main process for mass transport in very low water content argillites: 2. Fluid flow and mass transport modeling, Water Resources Research, 40, 2003WR002700, https://doi.org/10.1029/2003WR002700, 2004b.

Peltonen, C., Marcussen, Ø., Bjørlykke, K., and Jahren, J.: Clay mineral diagenesis and quartz cementation in mudstones: The effects of smectite to illite reaction on rock properties, Marine and Petroleum Geology, 26, 887–898, https://doi.org/10.1016/j.marpetgeo.2008.01.021, 2009.

Peyaud, J.-B., Barbarand, J., Carter, A., and Pagel, M.: Mid-Cretaceous uplift and erosion on the northern margin of the Ligurian Tethys deduced from thermal history reconstruction, Int J Earth Sci (Geol Rundsch), 94, 462–474, https://doi.org/10.1007/s00531-005-0486-z, 2005.

Pollastro, R. M.: Considerations and Applications of the Illite/Smectite Geothermometer in Hydrocarbon-Bearing Rocks of Miocene to Mississippian Age, Clays and Clay Minerals, 41, 119–133, https://doi.org/10.1346/CCMN.1993.0410202, 1993.

Robinet, J. C., Sardini, P., Siitari-Kauppi, M., Prêt, D., and Yven, B.: Upscaling the porosity of the Callovo-Oxfordian mudstone from the pore scale to the formation scale; insights from the 3H-PMMA autoradiography technique and SEM BSE imaging, Sedimentary Geology, 321, 1–10, https://doi.org/10.1016/j.sedgeo.2015.02.007, 2015.

Song, Y., Davy, C. A., Bertier, P., Skoczylas, F., and Talandier, J.: On the porosity of COx claystone by gas injection, Microporous and Mesoporous Materials, 239, 272–286, https://doi.org/10.1016/j.micromeso.2016.10.017, 2017.

Stahl, W. J.: Isotope geochemistry of light hydrocarbons adsorbed in Jurassic shales from the Hils syncline, Northwest Germany, in: Abhandlungen der Braunschweigischen Wissenschaftlichen Gesellschaft, vol. 43, Erich Goltze KG, Göttingen, 103–125, https://doi.org/https://doi.org/10.24355/dbbs.084-201308211449-0, 1993.

StandAG: Standortauswahlgesetz vom 5. Mai 2017 (BGBl. I S. 1074), das zuletzt durch Artikel 8 des Gesetzes vom 22. März 2023 (BGBl. 2023 I Nr. 88) geändert worden ist, https://www.gesetze-im-internet.de/standag_2017/, 2017.

Su, X., Nguyen, S., Haghighat, E., Pietruszczak, S., Labrie, D., Barnichon, J.-D., and Abdi, H.: Characterizing the mechanical behaviour of the Tournemire argillite, Geological Society, London, Special Publications, 443, 97–113, https://doi.org/10.1144/SP443.20, 2017.

Swarbrick, R. E. and Osborne, M. J.: Mechanisms that Generate Abnormal Pressures: An Overview, in: Abnormal Pressures in Hydrocarbon Environments, vol. 70, edited by: Law, B. E., Ulmishek, G. F., and Slavin, V. I., American Association of Petroleum Geologists, 0, https://doi.org/10.1306/M70615C2, 1998.

Tóth, E., Hrabovszki, E., Schubert, F., and Tóth, T. M.: Discrete fracture network (DFN) modelling of a high-level radioactive waste repository host rock and the effects on its hydrogeological behaviour, Journal of Structural Geology, 156, 104556, https://doi.org/10.1016/j.jsg.2022.104556, 2022.

Formatiert: Deutsch (Deutschland)

Totten, M. W., Hanan, M. A., Knight, D., and Borges, J.: Characteristics of mixed-layer smectite/illite density separates during burial diagenesis, American Mineralogist, 87, 1571–1579, https://doi.org/10.2138/am-2002-11-1207, 2002.

Van Geet, M., Bastiaens, W., and Ortiz, L.: Self-sealing capacity of argillaceous rocks: Review of laboratory results obtained from the SELFRAC project, Physics and Chemistry of the Earth, Parts A/B/C, 33, S396–S406, https://doi.org/10.1016/j.pce.2008.10.063, 2008.

Vandenberghe, N. and Mertens, J.: Differentiating between tectonic and eustatic signals in the Rupelian Boom Clay cycles (Lower Oligocene, Southern North Sea Basin), Newsletters on Stratigraphy, 46, 319–337, https://doi.org/10.1127/0078-0421/2013/0034, 2013.

Vogt, T., Hekel, U., Ebert, A., Becker, J. K., Traber, D., Giger, S., Brod, M., and Häring, C.: Hydrogeologische Untersuchungen im oberflächennahen Opalinuston (Bohrloch Lausen, Schweiz), Grundwasser, 22, 209–220, https://doi.org/10.1007/s00767-017-0363-2, 2017.

Voigt, T., Kley, J., and Voigt, S.: Dawn and dusk of Late Cretaceous basin inversion in central Europe, Solid Earth, 12, 1443–1471, https://doi.org/10.5194/se-12-1443-2021, 2021.

Voltolini, M. and Ajo-Franklin, J. B.: The Sealing Mechanisms of a Fracture in Opalinus Clay as Revealed by in situ Synchrotron X-Ray Micro-Tomography, Front. Earth Sci., 8, 207, https://doi.org/10.3389/feart.2020.00207, 2020.

Wagner, J.-F.: Mechanical Properties of Clays and Clay Minerals, in: Developments in Clay Science, vol. 5, Elsevier, 347–381, https://doi.org/10.1016/B978-0-08-098258-8.00011-0, 2013.

Wan, M., Delage, P., Tang, A. M., and Talandier, J.: Water retention properties of the Callovo-Oxfordian claystone, International Journal of Rock Mechanics and Mining Sciences, 64, 96–104, https://doi.org/10.1016/j.ijrmms.2013.08.020, 2013.

Wang, C., Talandier, J., and Skoczylas, F.: Swelling and Fluid Transport of Re-sealed Callovo–Oxfordian Claystone, Rock Mech Rock Eng, 55, 1143–1158, https://doi.org/10.1007/s00603-021-02708-4, 2022a.

Wang, C., Song, Y., Briffaut, M., Talandier, J., and Skoczylas, F.: Water Permeability and Swelling Characteristics of Callovo-Oxfordian Claystone: Summary of Laboratory Studies on Intact and Cracked Samples, Rock Mech Rock Eng, 58, 3227–3243, https://doi.org/10.1007/s00603-024-04283-w, 2025.

Wang, H., Cui, Y.-J., Vu, M. N., Talandier, J., and Conil, N.: Fracture effect on the hydro-mechanical behaviour of Callovo-Oxfordian claystone, Engineering Geology, 303, 106674, https://doi.org/10.1016/j.enggeo.2022.106674, 2022b.

Wang, H., Sun, Q., Pei, H., Zhang, Y., Vu, M.-N., Zhang, C., and Zhang, J.: Time-dependent permeability of fractured Callovo-Oxfordian claystone in laboratory and in situ drift excavation induced damaged zone in the claystone formation: experiment and numerical modeling, Bull Eng Geol Environ, 83, 53, https://doi.org/10.1007/s10064-024-03543-x, 2024.

Wemaere, I., Marivoet, J., and Labat, S.: Hydraulic conductivity variability of the Boom Clay in north-east Belgium based on four core drilled boreholes, Physics and Chemistry of the Earth, Parts A/B/C, 33, S24–S36, https://doi.org/10.1016/j.pce.2008.10.051, 2008.

Wersin, P., Mazurek, M., Waber, H. N., Mäder, U. K., Gimmi, T., Rufer, D., and de Haller, A.: Rock and porewater characterisation on drillcores from the Schlattingen borehole, Arbeitsbericht, NAB 12-54, Nagra, Wettingen, https://www.nagra.ch/reports/arbeitsbericht-nab-12-54, 2013.

Wersin, P., Aschwanden, L., Camesi, L., Gaucher, E. C., Gimmi, T., Jenni, A., Kiczka, M., Mäder, U., Mazurek, M., Rufer, D., Waber, H. N., Zwahlen, C., and Traber, D.: Dossier VIII Rock Properties, Porewater Characterisation and Natural Tracer Profiles, NAB 21-21, Nagra, Wettingen, https://www.nagra.ch/reports/arbeitsbericht-nab-21-21, 2022.

Formatiert: Deutsch (Deutschland)

Wetzel, A., Allenbach, R., and Allia, V.: Reactivated basement structures affecting the sedimentary facies in a tectonically "quiescent" epicontinental basin: an example from NW Switzerland, Sedimentary Geology, 157, 153–172, https://doi.org/10.1016/S0037-0738(02)00230-0, 2003.

Wijesinghe, P., Littke, R., Burnaz, L., Blumenberg, M., Erbacher, J., Mann, T., Amann, F., and Bauersachs, T.: Black shale deposition during the Early Jurassic: Geochemistry of Pliensbachian and Toarcian sedimentary rocks of the Hunzen Well, Hils Syncline, Northwest German Basin, The Depositional Record, 11, 1451–1478, https://doi.org/10.1002/dep2.70037, 2025.

Winhausen, L., Amann-Hildenbrand, A., Fink, R., Jalali, M., Khaledi, K., Hamdi, P., Urai, J. L., Schmatz, J., and Amann, F.: A comparative study on methods for determining the hydraulic properties of a clay shale, Geophysical Journal International, 224, 1523–1539, https://doi.org/10.1093/gji/ggaa532, 2020.

Winhausen, L., Khaledi, K., Jalali, M., Urai, J. L., and Amann, F.: Failure mode transition in Opalinus Clay: a hydro-mechanical and microstructural perspective, Solid Earth, 13, 901–915, https://doi.org/10.5194/se-13-901-2022, 2022.

Yang, Y. and Aplin, A. C.: Permeability and petrophysical properties of 30 natural mudstones, J. Geophys. Res., 112, 2005JB004243, https://doi.org/10.1029/2005JB004243, 2007.

Yu, C., Matray, J.-M., Gonçalvès, J., Jaeggi, D., Gräsle, W., Wieczorek, K., Vogt, T., and Sykes, E.: Comparative study of methods to estimate hydraulic parameters in the hydraulically undisturbed Opalinus Clay (Switzerland), Swiss J Geosci, 110, 85–104, https://doi.org/10.1007/s00015-016-0257-9, 2017.

Yu, L., Gedeon, M., Wemaere, I., Marivoet, J., and De Craen, M.: Boom Clay Hydraulic Conductivity A synthesis of 30 years of research, SCK-CEN-ER-122, SCK-CEN, Mol, Belgium, https://researchportal.sckcen.be/en/publications/boom-clay-hydraulic-conductivity-a-synthesis-of-30-years-of-resea/, 2011.

Yu, L., Rogiers, B., Gedeon, M., Marivoet, J., Craen, M. D., and Mallants, D.: A critical review of laboratory and in-situ hydraulic conductivity measurements for the Boom Clay in Belgium, Applied Clay Science, 75–76, 1–12, https://doi.org/10.1016/j.clay.2013.02.018, 2013.

Yven, B., Sammartino, S., Geraud, Y., Homand, F., and Villieras, F.: Mineralogy, texture and porosity of Callovo-Oxfordian argillites of the Meuse/Haute-Marne region (eastern Paris Basin), Mém. Soc. géol. France, 2007.

Zeelmaekers, E., Honty, M., Derkowski, A., Środoń, J., De Craen, M., Vandenberghe, N., Adriaens, R., Ufer, K., and Wouters, L.: Qualitative and quantitative mineralogical composition of the Rupelian Boom Clay in Belgium, Clay Minerals, 50, 249–272, https://doi.org/10.1180/claymin.2015.050.2.08, 2015.

Zhang, C.-L.: Experimental evidence for self-sealing of fractures in claystone, Physics and Chemistry of the Earth, Parts A/B/C, 36, 1972–1980, https://doi.org/10.1016/j.pce.2011.07.030, 2011.

Zhang, C.-L. and Talandier, J.: Self-sealing of fractures in indurated claystones measured by water and gas flow, Journal of Rock Mechanics and Geotechnical Engineering, 15, 227–238, https://doi.org/10.1016/j.jrmge.2022.01.014, 2023.

Zhang, C.-L., Wieczorek, K., and Xie, M. L.: Swelling experiments on mudstones, Journal of Rock Mechanics and Geotechnical Engineering., 2, 44–51, https://doi.org/https://doi.org/10.3724/SP.J.1235.2010.00044, 2010.

Zimmerli, G. N., Wohlwend, S., Deplazes, G., Becker, J., Wetzel, A., Francescangeli, F., and Foubert, A.: Facies variability and depositional cyclicity in central Northern Switzerland: insights from new Opalinus Clay drill cores, Swiss J Geosci, 117, 18, https://doi.org/10.1186/s00015-024-00463-6, 2024.